The serine protease homologue, Scarface, is sensitive to nutrient availability and modulates the development of the *Drosophila* blood brain barrier

Esteban G. Contreras[1*], Álvaro Glavic[2], Andrea H. Brand[3] and Jimena Sierralta[1*].

[1]Biomedical Neuroscience Institute and Department of Neuroscience, Faculty of Medicine, Universidad de Chile, Independencia 1027 Santiago-Chile, 8380453.

[2]FONDAP Center for Genome Regulation, Faculty of Science, Universidad of Chile, Las Palmeras 3425 Nuñoa, Santiago-Chile, 7800024.

[3]The Gurdon Institute and Department of Physiology, Development and Neuroscience, University of Cambridge, Tennis Court Road, Cambridge CB2 1QN, United Kingdom.

* Corresponding authors: Esteban G. Contreras (eocontre@uc.cl)
Jimena Sierralta (jsierral@uchile.cl)

Number of pages: 46

Number of figures: 11

Word Count: Abstract (249), Introduction (670), Discussion (1,636)

Conflict of interest statement: The authors declare no competing financial interests

Short title: Scarface modulates blood-brain growth

Key Words: *Drosophila melanogaster*, nutrient restriction, targeted DamID, blood-brain barrier, serine protease homologue, Scarface, subperineurial glia, perineurial glia, glial cells.

Acknowledgments: We would like to thank all the members of the Brand lab for their help during TaDa dissections. We thank S. Cheetham and R. Krautz for advice during library preparation and data analysis; P. Spéder and S. Noselli for anti-Scaf antibody and fly stocks; P. Olguín, F. Nuñez and G. Olivares for their support with the DAM2 system; C. Klämbt and B. Winkler for fly injection advice; the Bloomington *Drosophila* stock center and the Vienna *Drosophila* Resource Center (VDRC) for fly stocks; and the Developmental Studies Hybridoma Bank for antibodies. This work was supported by the Royal Society Darwin Trust Research Professorship and Wellcome Trust Senior Investigator Award 103792 (A.H.B.), ICMP09015F (J.S.), FONDECYT-Regular 1171800 (J.S.), FONDAP CGR 15090007 (A.G) and CONICYT PIA grant ACT1401 (J.S. and A.G.). A.H.B acknowledges core funding to The Gurdon Institute from the Wellcome Trust (092096) and CRUK (C6946/A14492).

Abstract

The adaptable transcriptional response to changes in food availability not only ensures animal survival, but also lets progressing with embryonic development. Interestingly, the central nervous system is preferentially protected to periods of malnutrition, a phenomenon known as '*brain sparing*'. However, the mechanisms that mediates this response remains poorly understood. To get a better understanding of this, we used *Drosophila melanogaster* as a model, analysing the transcriptional response of neural stem cells (neuroblasts) and glia of the blood-brain barrier (BBB), from larvae of both sexes, during nutrient restriction using targeted DamID. We found differentially expressed genes in both neuroblasts and glia of the BBB, although the effect of nutrient deficiency was primarily observed in the BBB. We characterised the function of a nutritional sensitive gene expressed in the BBB, the serine protease homologue, *scarface* (*scaf*). Scaf is expressed in subperineurial glia in the BBB in response to nutrition. Tissue-specific knockdown of *scaf* increases subperineurial glia endoreplication and proliferation of perineurial glia in the blood-brain barrier. Furthermore, neuroblast proliferation is diminished upon *scaf* knockdown in subperineurial glia. Interestingly, re-expression of Scaf in subperineurial glia is able to enhance neuroblast proliferation and brain growth of animals in starvation. Finally, we show that loss of *scaf* in the blood-brain barrier increases the sensitivity to drugs in adulthood suggesting a physiological impairment. We propose that Scaf integrates the nutrient status to modulate the balance between neurogenesis and growth of the BBB, preserving the proper equilibrium between the size of the barrier and the brain.

Significance Statement

The *Drosophila* Blood-brain barrier (BBB) separates the central nervous system from the open circulatory system. The BBB glia is not only acting as physical segregation of tissues but participates in the regulation of the metabolism and neurogenesis during development. Here we analyse the transcriptional response of the BBB glia to nutrient deprivation during larval development, a condition in which protective mechanisms are switched on in the brain. Our findings show that the gene *scarface* reduces growth in the BBB, while promoting the proliferation of neural stem, assuring the balanced growth of the larval brain. Thus, Scarface would link animal nutrition with brain development, coordinating neurogenesis with the growth of the BBB.

Introduction

The formation of the nervous system is a tightly regulated process that is controlled by complex mechanisms that mitigate external perturbations, such as temperature changes and food availability. For example, the developing mammalian brain is protected against intrauterine growth restriction by a phenomenon known as '*brain sparing*', in which the animal adapts to maintain oxygen and nutrient levels in the brain (Cohen et al., 2015). Brain development and function requires a micro-environment that is established and maintained by the blood-brain barrier (BBB), a selective barrier that separates the nervous system from the circulating blood. Therefore, the BBB could act as a metabolic sensor to protect the nervous system against a decrease in nutrient availability.

The mammalian BBB is established by endothelial cells forming tight junctions that prevent the paracellular diffusion of macromolecules and ions. Pericytes and astrocyte projections modulate the function of the BBB (Zhao et al., 2015; Gürsoy-özdemir and Tas, 2017; Haddad-Tóvolli et al., 2017), creating a selective barrier and establishing an homeostatic milieu independent from the rest of the body. The insect BBB covers the entire nervous system to isolate it from the haemolymph (the insect blood) (Carlson et al., 2000), and performs similar functions to the mammalian BBB. In insects, the BBB is formed by two layers of glia, perineurial and subperineurial (PG and SPG) (Awasaki et al., 2008; Stork et al., 2008; Hindle and Bainton, 2014; Schirmeier and Klämbt, 2015; O'Brown et al., 2018; Yildirim et al., 2019). The PG form the outer layer of the BBB, which regulates the transport of nutrients and secretes components of the extracellular matrix (the neural lamella) (DeSalvo et al., 2014; Volkenhoff et al., 2015; Kanai et al., 2018). The inner layer, the SPG, forms septate junctions that block the passive movement of solutes across the BBB (Baumgartner et al., 1996; Carlson et al., 2000; Schwabe et al., 2005; Stork

et al., 2008), controlling nutrient entry (Galagovsky et al., 2018) and the excretion of xenobiotic molecules (Tapadia and Lakhotia, 2005; Mayer et al., 2009; Hindle et al., 2017).

During development, the BBB not only acts as a barrier, but also influences the rate of neurogenesis by secreting growth factors that stimulate neurogenesis (Zhu et al., 2008; Chell and Brand, 2010; Sousa-Nunes et al., 2011; Spéder and Brand, 2014; Kanai et al., 2018). BBB glia mediates the reactivation of neural stem cells (neuroblasts, NB) from a period of quiescence in response to nutrition (Britton and Edgar, 1998; Chell and Brand, 2010; Sousa-Nunes et al., 2011). Periods of starvation during early larval development block neurogenesis by arresting NBs in a quiescent state. However, by third instar larval stages, NB are insensitive to undernourishment and continue proliferating, even after complete starvation, a phenomenon that resembles mammalian '*brain sparing*' (Cheng et al., 2011; Lanet et al., 2013; Lanet and Maurange, 2014; Contreras et al., 2018). This protocol of complete starvation is very effective in reducing the levels of carbohydrates, amino acids and proteins in the larval haemolymph (Cheng et al., 2011; Handke et al., 2013; Yamada et al., 2018). Considering this, it is plausible that the initial response of the central nervous system to the decrease in systemic nutrients is triggered by the BBB glia. Therefore, understanding how BBB gene expression is modulated by nutrition may yield insights into the adaptive mechanisms that govern brain sparing.

Here, we performed cell-type-specific transcriptional analysis of the BBB glia under fed and nutrient restriction (NR) conditions. Among the differentially expressed genes in the SPG, we found *scarface* (*scaf*), a member of the serine protease homologue (SPH) family. We show that *scaf* expression is sensitive to nutrition during larval development. *scaf* is expressed by the SPG and is required for controlling SPG growth and PG proliferation. Moreover, Scaf is necessary for proper rate of neurogenesis and its over-expression enhances NB proliferation and brain growth in

animals subjected to NR. Finally, we show that knocking down *scaf* in SPG affects the resistance of flies to drugs, suggesting that the function of the BBB is impaired when *scaf* is lost.

Material and Methods

Fly stocks and husbandry

Drosophila melanogaster stocks were cultured in fly food medium at 25°C. Our fly food contains the following ingredients per litre of medium: 100 g yeast, 80 g glucose, 50 g wheat flower, 11 g agar, 6 mL propionic acid, 12 mL 20% Nipagin (Methylparaben). All RNAi experiments were performed at 29°C.

For Targeted DamID (TaDa) analysis, we used *tub-GAL80^{ts}*, *UAS-LT3-NDam-RpII215* (*NDam-PolII*) and *tub-GAL80^{ts}*, *UAS-LT3-NDam* (Southall et al., 2013) crossed to the drivers *wor-GAL4* (Albertson et al., 2004), *mdr65*/*R54C07-GAL4* (Jenett et al., 2012; Spéder and Brand, 2014) or *sema5c/R71C08-GAL4* (Jenett et al., 2012). For functional experiments we used *w^{1118}* as experimental control, *UAS-shScaf^{RNAi}* (VDRC #330286), *UAS-lhScaf^{RNAi}* (VDRC #13249), *UAS-DlgA::EGFP* (Koh et al., 1999), *UAS-GFP.nls* (Kyoto DGGR #107-870), *UAS-mCD8-GFP*, *UAS-mCD8-RFP*, *UAS-lam:GFP* (BDSC #7378), *UAS-Scaf::GFP* (Rousset et al., 2010). For fluorescent reporters and fusion proteins we used the stocks: *scaf^{PBss}* (Scaf::GFP) (Bonin and Mann, 2004), *10xSTAT92E-GFP* (Bach et al., 2007), *TRE-RFP* (Chatterjee and Bohmann, 2012), *LanA::GFP* (VDRC #318155), *Lac::GFP^{G00044}* (Morin et al., 2001), *mdr65-mtdTomato* (Benmimoun et al., 2020). We used the glial drivers *R54C07-GAL4* (*mdr65-GAL4*, BDSC #50472) and *moody-GAL4* (Schwabe et al., 2005) for knockdown and overexpression experiments. We used the mutant alleles *scaf^{27}* (Rousset et al., 2010) and *scaf^{MI09409}* (Bloomington #53101).

Nutrient restriction protocol

Nutrient restriction (NR) experiments were performed as previously described (Contreras et al., 2018). Briefly, 68-72 hrs after larval hatching (ALH), larvae were transferred to a tube with fly food (Fed) or 1% Agarose in 1x PBS (NR). Tubes were left at 25°C for 24 hrs or until pupariation. For adult dissection, pupae were transferred to food tubes and adult fly brains were dissected 1-3 days after eclosion.

Sample collection for Targeted DamID

Briefly, we crossed *tub-GAL80^{ts}; UAS-LT3-NDam* and *tub-GAL80^{ts}; UAS-LT3-NDam- RpII215* to the respective drivers. We collected embryos for 3 hrs and let them develop for eight days at 18°C. Third instar larvae were transferred to 29°C for 1 day to induce the expression of the TaDa construct in either Fed or NR (1% Agarose, 1x PBS) conditions. 50-70 brains of each condition were dissected to extract genomic DNA. 2-5 replicates were processed.

DamID sequencing, processing and data analysis

The isolated genomic DNA from each cross was digested and amplified to generate libraries for next-generation sequencing as described (Marshall et al., 2016). Libraries were sequenced in an Illumina HiSeq 1500 with at least 8 million reads per library.

TaDa reads were aligned to *Drosophila melanogaster* genome release dm6 and normalised using the damidseq pipeline (Marshall and Brand, 2015). Genome browser views of bedgraph files were displayed as Log_2(DamPolII/Dam) using Integrative genomics viewer software (Robinson et al., 2011). PolII bound genes were called using the polii.gene.call R script (Marshall and Brand, 2015; Marshall et al., 2016) using *Drosophila* genome release annotation dm6.06. Genes with a

False Discovery Rate (FDR) lower than 0.01 were considered as bound by PolII. All genes from two datasets were compared using polii.correlation.plot R script (Marshall and Brand, 2015). Differentially bound genes have a difference between Log_2(Dam-PolII/Dam) values of 0.3, a FDR < 0.01 in at least one dataset, and a ratio of PolII binding bigger than 2. Student's T was used to analyse p-values between Fed and NR replicates.

Gene Ontology analysis of differentially expressed genes was performed using DAVID Bioinformatics Resources 6.8 (Huang et al., 2009a, 2009b). Association networks were done using String (Szklarczyk et al., 2019). Plots and heatmaps using custom R scripts are available upon request. PolII average Log_2(Dam-PolII/Dam) from each replicate were correlated using Pearson method and displayed as a heatmap using R gplots library. Volcano plots were generated using R ggplot2 library, Student's-T p-values were used to compare every replicate from two conditions (Fed and NR) and the difference of Log_2(Dam-PolII/Dam) for each gene in the conditions. Heatmaps were done using R pheatmap library and clustering genes using hclust complete method.

Data availability

DamID-Seq data was deposited in the Gene Expression Omnibus under the accession number GSE145055.

Immunostaining

Third instar larval brains were fixed in 4% formaldehyde for 20 min and stained as previously described (Wu and Luo, 2006). The following primary antibodies were used: rat anti-CadN 1:20 (DN-Ex #8, DSHB), guinea pig anti-Dpn 1:5,000 (Brand lab), rat anti-Elav 1:20 (7E8A10, DSHB),

mouse anti-Fas2 1:20 (1D4, DSHB), rabbit anti-phospho-Histone H3 1:400 (06-570 Merck), rat anti-phospho-Histone H3 1:500 (HTA28, Abcam), mouse anti-Repo 1:20 (8D12, DSHB), rabbit anti-Scaf N°2 1:200 (Rousset et al., 2010). DNA was stained using TO-PRO™-3 1:400 (T3605, Invitrogen) or 0.2 µg/mL DAPI. FITC, Cy3 or Cy5 conjugated secondary antibodies were used at a final concentration of 1:200 (Jackson ImmunoResearch).

For BBB permeability assays, larvae were opened at the tail and inverted, exposing the brain. Larvae were incubated with 20 µg/mL Rhodamine-Dextran 10,000 MW (Invitrogen, D1863) in Schneider's insect medium for 30 min at room temperature. Brains were washed in 1x PBS and fixed in 4% Formaldehyde in 1x PBS for 20 min. Samples were washed in PBT (0.3% Triton X-100, 1x PBS). Brains were dissected and mounted in Vectashield (Vector). For adult animals, males were anesthetised with CO_2, and approximately 60 nL of 12.5 µg/mL Rhodamine-Dextran 10,000 MW was injected in the abdomen using a Nanoject II Auto-Nanoliter Injector (Drummond Scientific Company). Flies were left to recover 2 hrs at room temperature and brains were dissected and fixed.

Imaging

Images were acquired using a Leica SP8 or an Olympus Fluoview FV1000 scanning confocal microscopes. Images of wings, pupae and adult flies were taken using a Nikon stereomicroscope with a Canon Rebel 2 Ti camera. Images, diagrams and figures were assembled using Fiji, Adobe Photoshop CC and Adobe Illustrator CC.

Behavioural Assays

Larval locomotion was performed by placing 10-12 larvae on a 1% agarose plate and recording a video for 1-2 minutes. Speed was calculating using Image J plugin wrMTrck (Brooks et al., 2016). Adult climbing was performed using a six-tube Counter-current apparatus (Inagaki et al., 2010). Briefly, groups of 15-30 female flies were placed in the first tube of the apparatus and allowed to climb for 30 seconds. Flies that climbed were transferred to the next tube and the process was repeated until the last tube was occupied. Then the number of flies in each tube was counted. The climbing index was calculated with the following equation: $Ci=(N_2+2N_3+3N_4+4N_5+5N_6)/5(N_1+N_2+N_3+N_4+N_5+N_6)$, in which N_1-N_6 corresponds to the number of flies in each of the six tubes. 8 different groups of flies were tested for each genotype. For fly activity and sleep assay, we used *Drosophila* Activity Monitors (DAM2, TriKinetics) and loaded adult flies following a previously described protocol (Chiu et al., 2010). Activity monitors were placed in an incubator with a 12:12 hrs light:dark cycle at 25°C for six days, only the last four days were used for data collection. The data were analysed using ShinyR-DAM (Cichewicz and Hirsh, 2018). Sleep was defined as inactivity in a period of 5 min.

For ethanol sedation sensitivity assay, we used groups of 8-10 male flies, placed in an empty vial with a cellulose acetate plug. 1 mL of ethanol was added to the plug and the fraction of immobile flies was counted every min until all flies were sedated (Sandhu et al., 2015). The time at which half the flies were sedated or sedation time 50 (ST50) was estimated by fitting a sigmoidal curve. For malathion resistance assay, we placed groups of 20 female flies in tubes containing 0.5 g of instant dry food (Carolina Biological Supply Company) and 2 mL 0.01% malathion in dH_2O. Lethality was counted at 12, 24 and 36 hrs after malathion exposure.

Quantifications and data analysis

Pupal volume was estimated as previously described (Layalle et al., 2008), using the ellipsoid volume formula $4/3\pi(L/2)(d/2)^2$ (L, length; d, diameter). Time of pupariation analysis was performed as we previously published (González-Itier et al., 2018). Larval and adult brain size was estimated using Imaris 7 (Bitplane) as described (Contreras et al., 2018). Neuropil size was estimated using the area of CadN staining in a maximal intensity Z-projection. SPG nuclear area was measured by generating a Z-stack max intensity projection and calculating the area of each SPG nucleus using Fiji (Li et al., 2017). The number of SPG nuclei was counted in a 3D reconstruction using Surpass feature of Imaris 7 (Bitplane). Number of PG was counted using *mdr65-GAL4, UAS-DlgA::GFP* or *moody-GAL4, UAS-GFP.nls* to mark SPG nuclei. Repo-positive/GFP-negative nuclei at the anterior surface of larval brain lobes were counted as PG. Scaf intensity was quantified by selecting the BBB optical slice, marking a ROI of the brain lobe and calculating the mean intensity of the Scaf channel using Fiji. For analysing the size of the wings, adult flies, 2-3 days after eclosion, were fixed in 95% ethanol for 24 hrs. Wings were dissected and mounted in a 1:1 lactic acid:ethanol solution. Fiji was used to measure the area of each wing.

All diagrams and figures were assembled using Fiji, Adobe Photoshop CC and Adobe Illustrator CC. Graphs and statistical analysis were done using GraphPad Prism 8. Description of each statistical test used is detailed in figure legends. P-values < 0.05, <0.01, <0.001 and <0.0001 are shown in plots as *, **, *** and **** respectively. ns stands for non-significant (p-value > 0.05).

Results

A *Drosophila* brain sparing model for understanding the response to nutrient restriction

To understand the transcriptional response of the *Drosophila* blood-brain barrier (BBB) to nutrient restriction (NR), we established the '*brain sparing*' model (Cheng et al., 2011; Contreras et al., 2018) under the temperature conditions required for performing PolII Targeted DamID (TaDa) (Southall et al., 2013). Thus, we allowed development at 18°C until 6 days after larval hatching (ALH) and switched to Fed or NR conditions at 29°C for 1 day (Figure 1A).

Following this protocol, the consequences of NR during larval development could be observed as a reduction in the size of the animal in both pupal (Figure 1F-H) and adult (Figure 1I-L) stages. The average size of the pupa after NR (pupal size reflects the maximum size that a larva reached before pupariation) corresponded to 34.51% of Fed animals (Figure 1H). We found that under this condition, larval brains continued growing upon NR, but not at the same rate as their Fed counterparts (Figure 1B-D). For the adult brain, we observed a significant reduction in the brain size of animals that were subjected to NR during larval development (Figure 1M, N). The larval and adult brains of NR animals reached 67.08% and 60.62% of the size of the Fed brains respectively (Figure 1E, O). Therefore, we were able to replicate the '*brain sparing*' effect under the conditions required to perform TaDa since the effect of NR over the growth of the whole animal was greater compared to the brain (body reduction to almost 35% compared to brain reduction to a 67 % of the Fed animal), reflecting the preferential growth of the nervous system during starvation (Cheng et al., 2011).

Transcriptional profiling of neuroblasts and blood-brain barrier glial cells under nutrient restriction

To determine the transcriptional response of neuroblasts and the BBB to NR, we profiled *in vivo,* and in a cell-type-specific manner, the binding of RNA Polymerase II (RpII215/PolII) using the TaDa technique. Briefly, TaDa uses the GAL4 system (Brand and Perrimon, 1993) to drive expression of a DNA binding or chromatin factor fused to the *E. coli* Dam methylase (Southall et al., 2013; Aughey and Southall, 2016; van den Ameele et al., 2019) (Figure 2-1A, B). We used two GAL4 drivers to target NDam-PolII expression in the SPG (*R54C07-GAL4*, also referred as *mdr65-GAL4*) or the PG and SPG together (SG, *R71C08-GAL4*, *sema5c-GAL4*, see Figure 2B-B'' for driver expression, and Figure 2-1D-G for PolII binding in BBB genes), and *wor-GAL4* for profiling NDam-PolII binding in all NBs (see Figure 2-1 and Figure 2A for a schematic representations). We performed TaDa under two nutritional conditions, Fed and NR, according to our established protocol (Figure 1A).

Meta-analysis of our PolII occupancy data showed the characteristic profile of PolII binding across a gene (Southall et al., 2013) (Figure 2-1C). Our TaDa replicates also correlated with each other as expected, with higher correlation between libraries of the same cell type and lower when NBs were compared to glial cells (Figure 2C). Next, we analysed the data and selected genes that were differentially bound by PolII between Fed and NR conditions in each dataset, considering genes with a false discovery rate (FDR) lower than 0.01, a PolII binding ratio higher than 2 and a difference higher than 0.3 (Figure 2D-F, Figure 2-2). In the NB comparison, we found 14 genes upregulated and 246 genes downregulated after NR (Figure 2D, G, H). In the BBB, 12 genes were upregulated and 47 downregulated in SPG (Figure 2E, I); while in the SG datasets, PolII TaDa showed 44 genes upregulated and 12 genes downregulated in the NR compared to Fed

condition (Figure 2F, J). Importantly, our data showed that PolII binding to genes associated to the drivers used (*wor*, *mdr65* and *sema5c*) was not affected by NR in the corresponding experiment.

The '*brain sparing*' model in *Drosophila* was previously shown to maintain NB proliferation upon NR (Cheng et al., 2011). Our NB PolII TaDa Gene Ontology analysis showed that categories involved in ribosome, mitochondria and oxidative phosphorylation metabolism were significantly enriched in downregulated genes (Figure 2G and Figure 2-1H). This suggests that energy metabolism and protein synthesis were affected in neural stem cells during NR. However, we found no significant differences in the growth and proliferation of NBs between Fed and NR conditions (Figure 3A, B), confirming that NB division and neurogenesis were not disrupted by starvation during third instar larval development (Cheng et al., 2011). In addition to this, we analysed the neuropil of larval brains, finding that the relative size of the neuropil was increased in animals under NR (Figure 3C-E), suggesting an effect of starvation over neuropil and cell body proportions.

In our BBB TaDa datasets, we found a group of proteins, associated with the JNK and JAK/STAT signalling pathways, that were downregulated after NR (Figure 2-1I). These included *Matrix metalloproteinase 1* (*Mmp1*) (Uhlirova and Bohmann, 2006), *scarface* (*scaf*) (Rousset et al., 2010; Srivastava and Dong, 2015), *eiger* (*egr*, TNF homologue), *TGF-β activated kinase 1* (*Tak1*) and the JAK/STAT ligands *unpaired 1* (*upd1*), *unpaired 2* (*upd2*) and *unpaired 3* (*upd3*) (Figure 2I, J and Figure 2-1I). Therefore, we analysed whether the JAK/STAT and JNK pathways were active in the larval BBB and if their activity was modulated by larval nutrition. We used the *10xSTAT92E-GFP* (Bach et al., 2007) and *TRE-RFP* (Chatterjee and Bohmann, 2012) reporters to evaluate JAK/STAT and JNK pathway activity respectively. As expected, both reporters were expressed in the BBB during larval development, however, the expression of these reporters did

not change after nutrient restriction (Figure 3F-I'), suggesting that these signalling pathways in the BBB are insensitive (not responding) to the nutritional status of the animal.

Nutrient restriction affects the development of the *Drosophila* blood-brain barrier

Since NB growth and proliferation were not affected by NR, we hypothesised that the larval BBB might adapt to starvation, being the first layer of the brain to sense and respond to a decrease in nutrients in the larval haemolymph.

The two types of glial cells that form the BBB, the subperineurial (SPG) and perineurial (PG) glia have different mechanisms of growth. SPG grow by endoreplication resulting in polyploid cells (Unhavaithaya and Orr-Weaver, 2012), while PG proliferate, undergoing mitosis (Pereanu et al., 2005; Awasaki et al., 2008; Avet-Rochex et al., 2012). SPG endoreplication takes place by either endocycle or endomitosis (Unhavaithaya and Orr-Weaver, 2012; Øvrebø and Edgar, 2018). Therefore, we checked the SPG for endomitosis by counting the number of SPG nuclei in third instar larval brains subjected to NR. We found a significant reduction in the number of nuclei in SPG (Figure 4A) and a significant decrease in the percentage of multinucleated SPG (Figure 4B). Similarly, the distribution of SPG with multiple nuclei changed significantly from a median of two in Fed animals to one after NR (Figure 4C, D). Given that the size of the nucleus correlates highly with cellular size and DNA content (Frawley and Orr-Weaver, 2015), nuclear size was measured as an indicator of SPG endocycle. We found a significant reduction in average nuclear size after NR (Figure 4E). We also counted the number of PG upon NR to check PG proliferation and observed a reduction in PG proliferation (Figure 4F). These results confirmed a major effect of nutrition on the BBB glial cells: a reduction in SPG endoreplication and a decrease in PG proliferation after food deprivation.

A severe reduction in SPG endoreplication affects the maintenance of the subperineurial septate junctions, allowing paracellular diffusion inside the larval brain (Unhavaithaya and Orr-Weaver, 2012; Von Stetina et al., 2018). Therefore, we checked the integrity of SPG septate junctions after nutrient restriction using an endogenously tagged version of the septate junction structural protein *lachesin* (*lac::GFP*) (Morin et al., 2001). We found no major disruptions in the continuity of the septate junctions in larval brains under NR conditions (Figure 4G-H). To test further the integrity of the BBB, we assessed BBB permeability by incubating larval brains with rhodamine labelled dextran (10 kDa) and assayed for penetration inside the ventral nerve cord. Rhodamine-dextran did not enter the central nervous system and remained on top of the subperineurial layer, marked by *mdr65-GAL4, UAS-mCD8-GFP* (Figure 4I, J). These results suggest that the integrity of the larval BBB is not disrupted by larval NR, despite the reduction in BBB growth.

Scarface is expressed in subperineurial glia and is regulated by nutrient availability

Since the growth of the BBB is affected by NR, we focused on BBB genes that were differentially expressed as indicated by our TaDa analysis. Of those, we centred our interest on *scarface* (*scaf*), one of the most downregulated genes during NR in SPG (see Figure 2I and Figure 5A). Scaf belongs to the serine protease homologue (SPH) family (Ross et al., 2003; Bonin and Mann, 2004; Rousset et al., 2010; Sorrosal et al., 2010). Serine protease homologues resemble proteases but lack the amino acids required for enzymatic activity. Scaf controls epithelial polarity and morphogenesis during embryonic development and thorax formation, acting as a downstream target of the JNK pathway and it has been reported to be a secreted protein (Rousset et al., 2010; Sorrosal et al., 2010; Srivastava and Dong, 2015; Kushnir et al., 2017).

To validate that *scaf* was differentially expressed upon NR, we made use of a gene trap line (*scaf*^{PBss} allele, Scaf::GFP) (Bonin and Mann, 2004) and an antibody against Scaf (anti-Scaf) (Rousset et al., 2010). Although, the *scaf*^{PBss} is a semi-lethal allele, when used in heterozygosis it is a reliable tool for analysing *scaf* expression. We observed Scaf expression in glial cells at the surface of the larval brain, corresponding to the BBB (Figure 5B-B'' and 5D-D''). As predicted by TaDa, the levels of Scaf were reduced after NR (Figure 5C-C'' and 5E-E''). Intensity quantification of the Scaf signal showed a significant reduction of an average of 47.56% and 59.37% of the Scaf intensity of Fed animals (Scaf::GFP and anti-Scaf, respectively) (Figure 5F, G).

As predicted by our SPG TaDa analysis, Scaf co-localised with a SPG membrane marker (*mdr65-GAL4, UAS-mCD8-GFP*, Figure 5I-J'') at the surface of the brain, but not with NBs, labelled by Deadpan (Dpn) (Figure 5H). Interestingly, the Scaf signal appeared also on top of the SPG membrane marker in a 3D reconstruction (Figure 5K-K''). To confirm this, we used an endogenously tagged *Laminin A* (*LanA::GFP*) line to label the brain extracellular matrix (neural lamella) and a SG membrane marker (*sema5c-GAL4, UAS-mCD8-RFP*). Since the thickness of the BBB is about 2 µm, we observed that Scaf signal overlapped with LanA and most of SG membrane signals, thus the entire BBB (Figure 5L-L''). These results showed that during third instar larval development *scaf* is expressed by SPG in a nutrition-sensitive fashion (Figure 5M).

Scarface reduces the growth of the blood-brain barrier during larval development

Since SPG expression of Scaf is sensitive to nutrition, we aimed to assess its function in the BBB during normal development. To accomplish this, we performed RNAi-mediated knockdown of *scaf* only in SPG using the *mdr65-GAL4* driver. We tested two different RNAi lines, a short hairpin

(*shScaf*^{RNAi}) and a long hairpin (*lhScaf*^{RNAi}), finding that both were able to significantly reduce the levels of Scaf in the BBB (Figure 6A-D). Because *shScaf*^{RNAi} gave the most efficient knockdown (29.63% of control Scaf levels), we used this line in most of our experiments.

Knockdown of *scaf* in SPG produced normal larvae, which grew and pupariated as control animals, and emerged into fertile adult flies (Figure 6E-H). We checked the development of the BBB at late third instar larval stage, observing no morphological defects (Figure 6I, J). Thus, we analysed endomitosis of SPG, finding a significant increase in the number of SPG nuclei after *scaf* knockdown (Figure 6K), but without a significant change in the percentage of multinucleated SPG per brain lobe (Figure 6L). This suggested that upon *scaf* knockdown the number of multinucleated SPG is similar, but they contain more nuclei than in control animals. This was confirmed by analysing the distribution of SPG according to the number of their nuclei, showing an increase in the median from one nucleus in control animals to two nuclei in *shScaf*^{RNAi} brains (Figure 6M, N).

Next, we checked the nuclear size in SPG, observing a significant increase upon *scaf* knockdown (Figure 6O), which suggests an increase in SPG endocycle. We also found a significant increase in the number of PG in *shScaf*^{RNAi} animals (Figure 6P). We confirmed these results using the *lhScaf*^{RNAi} strain (see Figure 6-1). Next, we assessed whether permeability of the BBB was altered in *scaf* knockdown larval brains using the Rhodamine-dextran assay described before. We did not detect the colorant inside the central nervous system (Figure 6Q, R), ratifying that a reduction in the levels of Scaf increases the growth of the subperineurial layer as well as the number of PG, without affecting the BBB permeability.

Given that *scaf* knockdown augmented the growth of the BBB, increasing the levels of Scaf should produce the opposite effect. To perform gain of function experiments in SPG during development, we used a line (*UAS-Scaf*) that rescues *scaf* mutant embryonic lethality (Rousset et

al., 2010). Over-expression of Scaf generated normal and viable animals, without affecting larval growth under Fed or NR conditions, however, the timing of puparation was significantly accelerated (see Figure 7A-F). In the BBB, we found that the average number of SPG nuclei did not change upon Scaf over-expression (Figure 7G), however, the percentage of multinucleated SPG in a brain lobe was significantly decreased (Figure 7H). We also observed an increase in the mononucleated fraction of SPG, but without a change in the overall distribution (Figure 7I, J). Interestingly, the size of the SPG nuclei was significantly reduced by Scaf over-expression (Figure 7K). These results showed that increasing the levels of Scaf has a mild effect on SPG endoreplication. In the perineurial layer, the number of PG was not affected by Scaf over-expression (Figure 7L), suggesting that there was no impact on PG proliferation. Our data infer a role for Scaf in diminishing the growth of the BBB through decreasing the levels of SPG endocycle and endomitosis during development under normal nutritional conditions.

Blood-brain barrier-derived Scarface promotes neurogenesis in the larval brain

Nutrient restriction reduced the levels of Scaf in the BBB, and also produced animals with smaller brains than control Fed condition. We assessed whether Scaf function at the BBB has a non-autonomous effect on neurogenesis. Thus, we knocked down *scaf* in SPG and checked the mitotic index of larval central brain NBs, observing a significant decrease in the fraction of NBs in mitosis (Figure 8A-C). To confirm this result, we used a *scaf* allelic combination of $scaf^{27}$, a deletion resulting in a strong lethal allele (Rousset et al., 2010), with $scaf^{MI09409}$, a semi-lethal allele generated by a MiMIC insertion (Venken et al., 2011) producing a truncated Scaf protein (that retains the antibody epitope). This, $scaf^{27}/scaf^{MI09409}$ allelic combination is a hypomorphic condition that is viable and healthy during larval development, but lethal at late pupal stage.

Similar to *scaf* knockdown experiments, we found that *scaf* mutant brains had a significantly lower NB mitotic index than heterozygous animals ($scaf^{27/+}$) (Figure 8D). In the same way, the hypomorphic allelic combination, $scaf^{PBss}/scaf^{27}$, also showed a decreased NB mitotic index compared to the heterozygous control ($scaf^{PBss/+}$) (Figure 8E, G). Since *scaf* in the BBB was necessary for proper NB proliferation, we conducted a rescue experiment to determine whether the expression of Scaf only in SPG was sufficient to maintain the normal NB mitotic index in *scaf* mutant animals. As seen in Figure 8E, the over-expression of *scaf* was not able to rescue NB mitotic index in a *scaf* mutant background. Thus, Scaf from SPG is not sufficient to maintain NB proliferation in the mutant (Figure 8E). Additionally, the knockdown of *scaf* only in SPG did not have a major impact on the overall size of the brain (Figure 8F). These results suggest that Scaf is necessary in the BBB to maintain the rate of larval neurogenesis, but Scaf in other cell types is also required for NB proliferation.

As Scaf downregulation affects the rate of NB proliferation under normal nutritional conditions, we analysed whether Scaf over-expression in SPG could enhance neurogenesis in animals subjected to NR. We found that in NR conditions, expression of Scaf in SPG resulted in a 13.78% increase in the size of the adult brain in comparison to control NR animals (Figure 9A-C). Furthermore, the larval central brain NB mitotic index was also increased upon Scaf over-expression in animals under NR (Figure 9D). For the BBB, Scaf over-expression did not prevent the reduction in the growth of the SPG or PG layers during NR (Figure 9E-J). Importantly, we did not observe a difference in brain growth during normal Fed conditions upon Scaf over-expression (Figure 9K-M), showing that Scaf over-expression enhances brain growth only under starvation. In the case of the growth of other organs, re-expression of Scaf in the BBB during NR, induced a

small increase in the size of adult wings (4.76% of increase compared to control animals, see Figure 9N-R).

Taken together, these results demonstrate that Scaf, expressed by the SPG layer, is required for maintaining the rate of neurogenesis. This highlights a non-autonomous role for Scaf in coordinating neurogenesis and the growth of the BBB. Additionally, Scaf re-expression is able to promote brain growth during nutrient deprivation.

Drug sensitivity is increased upon *scarface* loss in the blood-brain barrier

We found that Scaf modulates the growth of the BBB and has a role in maintaining the rate of NB proliferation in the central brain. However, the loss of *scaf* seemed to have only a mild effect in the development of the central nervous system. Therefore, we wonder whether the phenotypes observed after *scaf* knockdown during larval development, impacts the function of the BBB and the central nervous system of the adult animal.

With this goal, we analysed locomotor activity in larval and adult animals upon *scaf* knockdown in SPG. We found no significant differences in the larval crawling speed (average and maximum) of control and *scaf* knockdown animals (Figure 10A, B). Similar results were obtained when we assessed climbing activity in adult flies (Figure 10C). As BBB function has been associated with circadian activity rhythm and sleep (Artiushin et al., 2018; Zhang et al., 2018; Cuddapah et al., 2019), we analysed locomotor activity and sleep in adult flies using *Drosophila* activity monitors (DAM2). We found no differences in total activity or activity profile between control and *scaf* knockdown groups (Figure 10D, F). Total sleep was not affected in *scaf* knockdown animals either (note that driver alone sleep did not differ from *scaf* knockdown group

in Figure 10E), however, the sleep profile of these animals showed less sleep than both control groups a few hours before the end of the light cycle (Figure 10G).

One of the major roles of the BBB is to control the efflux and influx of molecules across the brain and it is known that the sensitivity to different drugs is altered in mutant animals with defects in BBB permeability (Bainton et al., 2005; Mayer et al., 2009). The BBB permeability is controlled by preventing paracellular diffusion (by septate junctions) and by the active extrusion of lipophilic molecules into the haemolymph. Hence, we assessed the sensitivity to ethanol and malathion as a manner to test for BBB function defects. Ethanol, although attractive for the flies, produces incoordination and loss of equilibrium in flies (pass out), and its tolerance is regulated in the BBB by the action of A kinase anchoring protein (Akap200) in PG (Parkhurst et al., 2018). Malathion is an organophosphate insecticide that blocks acetylcholinesterase, inducing hyperexcitability since acetylcholine is the main excitatory neurotransmitter in the fly brain. In *Drosophila*, malathion sensitivity is increased by the loss of the ATP-binding cassette (ABC) transporter, *mdr65* (Sun et al., 2017), which is necessary for BBB xenobiotic efflux (Mayer et al., 2009; Hindle et al., 2017). Similarly, in vertebrates malathion can cross and affect the structure of the BBB (Balbuena et al., 2010, 2011). We found that sensitivity to a single exposure of ethanol was significantly enhanced in animals with *scaf* knockdown in SPG (Figure 11A, B) and animals exposed to malathion, showed a significant increase in lethality compared to control animals (Figure 11C). Interestingly, adult flies that were subjected to larval NR, in which *scaf* is downregulated in the BBB, also showed an increased sensitivity to ethanol (Figure 11D, E). Importantly, the sensitivity to drugs after *scaf* knockdown could not be attributed to an effect over the excretion of drugs, since *scaf* RNAi was not expressed in the adult gut or renal (Malpighian) tubules (see *mdr65-GAL4* expression in Figure 11F, G). Additionally, paracellular permeability of

491 the adult BBB was not affected by *scaf* knockdown (Figure 11H, I), suggesting that extrusion of
492 xenobiotic agents may be affected by the loss of *scaf* in the BBB.

493 These results show that reducing the expression of *scaf* in the BBB, which has an effect
494 over the BBB growth, increases the sensitivity of the central nervous system to exogenous agents,
495 supporting a role of Scaf in the regulation of the function of the BBB.

Discussion

The adaptive response of animals to periods of famine is essential for species survival. In the central nervous system, the brain is preferentially protected over other tissues during starvation. Here, we analyse the transcriptional response of *Drosophila melanogaster* neuroblasts (NBs) and blood-brain barrier (BBB) glial cells to nutrient restriction (NR) during larval development using PolII Targeted DamID (TaDa). Overall, we found differentially expressed genes in NBs, subperineurial and surface glial datasets. We also found that, in our starvation model, the major effect of NR was on the growth of the BBB. Thus, we focused on the function of a gene that is highly regulated by NR in the BBB; the serine protease homologue (SPH) *scarface* (*scaf*). We determined that *scaf* is expressed in the subperineurial glia (SPG) and its expression is modulated by the animal's nutritional state. Tissue-specific knockdown of *scaf* showed that it is required to restrict the growth of the BBB and to maintain a proper rate of NB proliferation. In accordance with this, reintroducing Scaf expression in SPG enhances neurogenesis in animals subjected to nutritional stress. Finally, we showed that *scaf* knockdown in the BBB increases the sensitivity to drugs in adult animals, suggesting defects in the control of the influx/efflux of molecules across the BBB.

A genetic response of the central nervous system to food scarcity

The maintenance of homeostasis during inanition permits animal survival and developmental progression. Among the different organs, the central nervous system, which is extremely sensitive to stress conditions, is protected from systemic nutrient reduction. The '*brain sparing*' model is good example of this mechanism of protection during development. In *Drosophila*, neural stem

cell proliferation depends on nutrition at early larval stages (Britton and Edgar, 1998; Chell and Brand, 2010; Sousa-Nunes et al., 2011), but it is independent of nutrition through the end of third instar larval stage (after acquiring the minimal viable weight) (Cheng et al., 2011). Cheng *et al.* described that NBs maintain their proliferation rate by the action of Jelly belly/Anaplastic lymphoma kinase that activates the phosphatidylinositol 3-kinase (PI3K) pathway. However, these pathways do not respond to starvation nor are they modulated by the nutritional state of the animal (Cheng et al., 2011). This raised the question of whether neural stem cells respond to, or are insensitive to, nutrient restriction. It is plausible that molecular adaptation to nutritional stress occurs in other cell types, such as glial cells, or in other organs.

Our TaDa data showed that there are transcriptional changes in NBs during NR that could help to maintain proliferation and neurogenesis. We postulate that the decrease in the expression of genes associated with ribosome and mitochondrial metabolism could help to maintain the rate of NB proliferation upon nutrient restriction. During pupal development, oxidative phosphorylation is required for NBs to reduce growth and exit the cell cycle (Homem et al., 2014; van den Ameele and Brand, 2019), but it is also necessary for larval NBs and NB-derived tumour proliferation (Genovese et al., 2019; van den Ameele and Brand, 2019). Hence, modulating mitochondrial metabolism could be a NB response for maintaining neurogenesis during nutrient restriction. However, the actual contribution of this metabolic regulation to neurogenesis is unknown.

On the other hand, it is well established that other organs contribute to the '*brain sparing*' phenomenon. For instance, upon starvation polyploid tissues such as salivary glands and fat body stop growing (Cheng et al., 2011), and fat body-derived glycogen maintains trehalose levels in the haemolymph (Yamada et al., 2018). Therefore, nutrient stores are mostly available for the central

nervous system to continue growing. The role of neurons and glial cells in this process is less understood. In the case of hypoxia, NB proliferation is protected by the formation of lipid droplets in glial cells (Bailey et al., 2015), supporting a protective role of glial cells. In recent work, the group of Simon Sprecher characterised the response of the first instar larval brain to starvation using single cell sequencing. Although, under these conditions neurogenesis is completely blocked, they found a transcriptional response in glial cells to promote lipid catabolism (Brunet Avalos et al., 2019). The glia forming the BBB are likely to be the first sensors of nutrient reduction in the haemolymph. The presence of different macromolecule transporters in the BBB (DeSalvo et al., 2014; Volkenhoff et al., 2015; Galagovsky et al., 2018) and their capacity to store neutral lipids (Bailey et al., 2015), supports the role of the BBB as the nutritional gatekeeper of the brain.

In our analysis, we observed that SPG showed an important transcriptional response to nutrient restriction. Among the differentially expressed genes, we found secreted proteins and components of the JNK and JAK/STAT signalling that are well-characterised stress-response pathways. Recently, Prasad and Hens analysed the transcriptional response of the adult brain to starvation and sugar absence, finding many secreted proteins, including serine protease homologues and Scaf secreted from a group of neurons (‘*scarface neurons*’ in the adult brain), which promote feeding behaviour (Prasad and Hens, 2018). Thus, it is plausible that changes in the expression of secreted proteins, including Scaf, are part of a signature of the brain response to nutrient restriction. Surprisingly, we found that the activity of the JNK and JAK/STAT pathways in the BBB was not affected by nutrient restriction. It would be interesting to evaluate whether during nutrient restriction, a decrease in components of these pathways behave as signals from the BBB to other tissues. This is possible considering that Unpaired cytokines and the TNF Eiger from

563 the fat body regulate homeostasis in a systemic manner, which also depends on nutrition (Rajan
564 and Perrimon, 2012; Agrawal et al., 2016).

565

566 **Scarface coordinates blood-brain barrier growth with neurogenesis in a cell non-**
567 **autonomous manner**

568 From our TaDa analysis we selected Scaf as a good candidate to mediate BBB adaptation to
569 nutrient restriction. Scaf belongs to the serine protease homologue (SPH) family that lacks amidase
570 activity (Ross et al., 2003; Bonin and Mann, 2004). Scaf was previously described to be a
571 transcriptional target of the JNK pathway that controls epithelial polarity and morphogenesis
572 during dorsal closure (Rousset et al., 2010; Sorrosal et al., 2010; Kushnir et al., 2017) and thoracic
573 development (Srivastava and Dong, 2015). We showed that Scaf expression in SPG depends on
574 nutrition and one of its roles is to reduce SPG growth by endocycle/endomitosis as well as PG
575 proliferation. Although, the effect of *scaf* loss is not strong to affect animal development to
576 adulthood, the sensitivity to drugs that cross the BBB is enhanced, revealing a physiological
577 consequence to this defect in the growth of the BBB. We postulate that loss of *scaf* could affect
578 transcellular diffusion of organic molecules across the BBB or the function of efflux transporters
579 that eliminate xenobiotics from the brain (Mayer et al., 2009; Hindle et al., 2017; Sun et al., 2017).

580 How Scaf regulates the growth of the BBB is unknown. As Scaf has been shown to be a
581 secreted protein (Rousset et al., 2010; Sorrosal et al., 2010), we propose that Scaf from SPG
582 modulates the activity of growth factors for both SPG and PG. The balance between SPG
583 endocycle and endomitosis is regulated by the Notch pathway (Von Stetina et al., 2018). This
584 mechanism seems to be an autocrine signalling, because Delta ligand is also necessary in SPG for
585 promoting endocycle over endomitosis (Von Stetina et al., 2018). On the other hand, PG

proliferates in response to Insulin and FGF signalling (Franzdóttir et al., 2009; Avet-Rochex et al., 2012). Therefore, it is possible that Scaf could affect these signalling pathways to reduce the growth of the BBB. Given that Scaf represses the JNK pathway during embryogenesis, it was postulated that Scaf could act on an unknown extracellular signal, including components of the extracellular matrix (Rousset et al., 2010). Spheroid, another SPH, regulates Toll pathway activation in a bacterial infection model (Patrnogic and Leclerc, 2017), whereas the SPH Masquerade regulates muscle attachment by stabilising cell-matrix interactions (Murugasu-Oei et al., 1995). We showed that Scaf reaches the entire BBB, therefore, Scaf may play a similar role in modulating signalling pathways in the BBB as other SPHs. Alternatively, Scaf could also have a role intracellularly since it can be found in early, late and recycling endosomes in neighbouring cells (Sorrosal et al., 2010).

Interestingly, Scaf displays a cell non-autonomous effect over NB proliferation. We did not detect Scaf in NBs, therefore, this effect is indirect. One possibility is that reducing BBB growth could impact on nutrients availability inside the brain. This could explain the fact that Scaf overexpression during nutrient restriction enhances brain growth. Similarly, a reduction in BBB growth, mediated by Scaf, could increase the secretion of growth factors such as Insulin-like peptides and Activin that control NB proliferation (Zhu et al., 2008; Chell and Brand, 2010; Sousa-Nunes et al., 2011). Additionally, its over-expression in the BBB did not rescue the proliferation effect observed in the mutants, suggesting that other glial cells, such as cortex glia, could be expressing Scaf and contributing to the neurogenic niche.

We believe that the decrease in Scaf levels is part of a highly complex mechanism to maintain growth in the BBB during NR. Knocking down *scaf* in the BBB does not completely recapitulate the phenotype observed during starvation, suggesting that other pathways are affected.

Moreover, re-expression of Scaf during NR does not rescue BBB growth. We propose that during normal development Scaf responds to nutrient availability and acts as a negative feedback over BBB growth, contributing to the fine-tuning of the balance between BBB growth and neurogenesis in the central nervous system. Upon larval starvation, this balance is lost, and neurogenesis is prioritised at the expense of the growth of the BBB. Future experimental evidence will be needed to unveil the molecular mechanisms by which Scaf supports this balance of growth during the development of the nervous system.

References

Agrawal N, Delanoue R, Mauri A, Basco D, Pasco M, Thorens B, Léopold P (2016) The Drosophila TNF Eiger Is an Adipokine that Acts on Insulin-Producing Cells to Mediate Nutrient Response. Cell Metab 23:675–684.

Albertson R, Chabu C, Sheehan A, Doe CQ (2004) Scribble protein domain mapping reveals a multistep localization mechanism and domains necessary for establishing cortical polarity. J Cell Sci.

Artiushin G, Zhang SL, Tricoire H, Sehgal A (2018) Endocytosis at the Drosophila blood–brain barrier as a function for sleep. Elife 7:1–18.

Aughey GN, Southall TD (2016) Dam it's good! DamID profiling of protein-DNA interactions. Wiley Interdiscip Rev Dev Biol 5:25–37.

Avet-Rochex A, Kaul AK, Gatt AP, McNeill H, Bateman JM (2012) Concerted control of gliogenesis by InR/TOR and FGF signalling in the Drosophila post-embryonic brain. Development 139:2763–2772.

Awasaki T, Lai S-L, Ito K, Lee T (2008) Organization and Postembryonic Development of Glial Cells in the Adult Central Brain of Drosophila. J Neurosci 28:13742–13753.

Bach EA, Ekas LA, Ayala-Camargo A, Flaherty MS, Lee H, Perrimon N, Baeg G-H (2007) GFP reporters detect the activation of the Drosophila JAK/STAT pathway in vivo. Gene Expr Patterns 7:323–331 Available at: https://www.sciencedirect.com/science/article/abs/pii/S1567133X06001566?via%3Dihub [Accessed November 11, 2019].

Bailey AP, Koster G, Guillermier C, Hirst EMA, MacRae JI, Lechene CP, Postle AD, Gould AP (2015) Antioxidant Role for Lipid Droplets in a Stem Cell Niche of Drosophila. Cell 163:340–353 Available at: http://dx.doi.org/10.1016/j.cell.2015.09.020.

Bainton RJ, Tsai LTY, Schwabe T, DeSalvo M, Gaul U, Heberlein U (2005) moody encodes two GPCRs that regulate cocaine behaviors and blood-brain barrier permeability in Drosophila. Cell 123:145–156.

Balbuena P, Li W, Ehrich M (2011) Assessments of tight junction proteins occludin, claudin 5 and scaffold proteins ZO1 and ZO2 in endothelial cells of the rat blood-brain barrier: Cellular responses to neurotoxicants malathion and lead acetate. Neurotoxicology 32:58–67 Available at: http://dx.doi.org/10.1016/j.neuro.2010.10.004.

Balbuena P, Li W, Magnin-Bissel G, Meldrum JB, Ehrich M (2010) Comparison of two blood-brain barrier in vitro systems: Cytotoxicity and transfer assessments of malathion/oxon and lead acetate. Toxicol Sci 114:260–271.

Baumgartner S, Littleton JT, Broadie K, Bhat MA, Harbecke R, Lengyel JA, Chiquet-Ehrismann R, Prokop A, Bellen HJ (1996) A Drosophila neurexin is required for septate junction and blood-nerve barrier formation and function. Cell 87:1059–1068 Available at: http://www.ncbi.nlm.nih.gov/pubmed/8978610 [Accessed June 23, 2019].

Benmimoun B, Papastefanaki F, Périchon B, Segklia K, Roby N, Miriagou V, Schmitt C, Dramsi S, Matsas R, Spéder P (2020) An original model of brain infection identifies the hijacking of host lipoprotein import as a bacterial strategy for blood-brain barrier crossing. Nat Commun Available at: http://dx.doi.org/10.1038/s41467-020-19826-2.

Bonin CP, Mann RS (2004) A piggyBac transposon gene trap for the analysis of gene expression and function in Drosophila. Genetics 167:1801–1811.

Brand AH, Perrimon N (1993) Targeted gene expression as a means of altering cell fates and generating dominant phenotypes. Development 118:401–415 Available at: http://www.ncbi.nlm.nih.gov/pubmed/8223268.

Britton JS, Edgar BA (1998) Environmental control of the cell cycle in Drosophila: nutrition activates mitotic and endoreplicative cells by distinct mechanisms. Development 125:2149–2158 Available at: http://www.ncbi.nlm.nih.gov/pubmed/9570778.

Brooks DS, Vishal K, Kawakami J, Bouyain S, Geisbrecht ER (2016) Optimization of wrMTrck to monitor Drosophila larval locomotor activity. J Insect Physiol.

Brunet Avalos C, Bruggmann R, Sprecher SG (2019) Single cell transcriptome atlas of the Drosophila larval brain.

660 Elife 8:1–25 Available at: https://elifesciences.org/articles/50354 [Accessed December 3, 2019].

661 Carlson SD, Juang J-L, Hilgers SL, Garment MB (2000) Blood Barriers of the Insect. Annu Rev Entomol 45:151–
662 174.

663 Chatterjee N, Bohmann D (2012) A versatile φC31 based reporter system for measuring AP-1 and NRF2 signaling in
664 Drosophila and in tissue culture. PLoS One 7.

665 Chell JM, Brand AH (2010) Nutrition-responsive glia control exit of neural stem cells from quiescence. Cell
666 143:1161–1173 Available at: http://dx.doi.org/10.1016/j.cell.2010.12.007.

667 Cheng LY, Bailey AP, Leevers SJ, Ragan TJ, Driscoll PC, Gould AP (2011) Anaplastic lymphoma kinase spares
668 organ growth during nutrient restriction in drosophila. Cell 146:435–447 Available at:
669 http://dx.doi.org/10.1016/j.cell.2011.06.040.

670 Chiu JC, Low KH, Pike DH, Yildirim E, Edery I (2010) Assaying locomotor activity to study circadian rhythms and
671 sleep parameters in Drosophila. J Vis Exp:1–9.

672 Cichewicz K, Hirsh J (2018) ShinyR-DAM: a program analyzing Drosophila activity, sleep and circadian rhythms.
673 Commun Biol 1:25 Available at: http://www.nature.com/articles/s42003-018-0031-9 [Accessed September 30,
674 2019].

675 Cohen E, Baerts W, Van Bel F (2015) Brain-Sparing in Intrauterine Growth Restriction: Considerations for the
676 Neonatologist. Neonatology 108:269–276.

677 Contreras EGEGEG, Sierralta J, Glavic A (2018) p53 is required for brain growth but is dispensable for resistance to
678 nutrient restriction during Drosophila larval development Missirlis F, ed. PLoS One 13:e0194344 Available at:
679 https://dx.plos.org/10.1371/journal.pone.0194344.

680 Cuddapah VA, Zhang SL, Sehgal A (2019) Regulation of the Blood-Brain Barrier by Circadian Rhythms and Sleep.
681 Trends Neurosci 42:500–510 Available at: http://www.ncbi.nlm.nih.gov/pubmed/31253251 [Accessed July 1,
682 2019].

683 DeSalvo MK, Hindle SJ, Rusan ZM, Orng S, Eddison M, Halliwill K, Bainton RJ (2014) The Drosophila surface glia
684 transcriptome: Evolutionary conserved blood-brain barrier processes. Front Neurosci 8:1–22.

685 Franzdóttir SR, Engelen D, Yuva-Aydemir Y, Schmidt I, Aho A, Klämbt C (2009) Switch in FGF signalling initiates
686 glial differentiation in the Drosophila eye. Nature 460:758–761.

687 Frawley LE, Orr-Weaver TL (2015) Primer Polyploidy. Curr Biol 25:353–358.

688 Galagovsky D, Depetris-Chauvin A, Manière G, Geillon F, Berthelot-Grosjean M, Noirot E, Alves G, Grosjean Y
689 (2018) Sobremesa L-type Amino Acid Transporter Expressed in Glia Is Essential for Proper Timing of
690 Development and Brain Growth. Cell Rep 24:3156-3166.e4.

691 Genovese S, Clément R, Gaultier C, Besse F, Narbonne-Reveau K, Daian F, Foppolo S, Luis NM, Maurange C (2019)
692 Coopted temporal patterning governs cellular hierarchy, heterogeneity and metabolism in Drosophila neuroblast
693 tumors. Elife 8:1–36 Available at: https://elifesciences.org/articles/50375.

694 González-Itier S, Contreras EGEGEG, Larraín J, Glavic Á, Faunes F (2018) A role for Lin-28 in growth and
695 metamorphosis in Drosophila melanogaster. Mech Dev 154:107–115 Available at:
696 https://doi.org/10.1016/j.mod.2018.06.002.

697 Gürsoy-özdemir Y, Tas YC (2017) Anatomy and Physiology of the Blood-Brain Barrier. Nanotechnol Methods
698 Neurol Dis Brain Tumors Drug Deliv across Blood-Brain Barrier 38:1–13.

699 Haddad-Tóvolli R, Dragano NRV, Ramalho AFS, Velloso LA (2017) Development and function of the blood-brain
700 barrier in the context of metabolic control. Front Neurosci 11:1–12.

701 Handke B, Poernbacher I, Goetze S, Ahrens CH, Omasits U, Marty F, Simigdala N, Meyer I, Wollscheid B, Brunner
702 E, Hafen E, Lehner CF (2013) The Hemolymph Proteome of Fed and Starved Drosophila Larvae. PLoS One
703 8:1–10.

704 Hindle SJ, Bainton RJ (2014) Barrier mechanisms in the Drosophila blood-brain barrier. Front Neurosci 8:1–12.

Hindle SJ, Munji RN, Dolghih E, Gaskins G, Orng S, Ishimoto H, Soung A, DeSalvo M, Kitamoto T, Keiser MJ, Jacobson MP, Daneman R, Bainton RJ (2017) Evolutionarily Conserved Roles for Blood-Brain Barrier Xenobiotic Transporters in Endogenous Steroid Partitioning and Behavior. Cell Rep 21:1304–1316 Available at: https://doi.org/10.1016/j.celrep.2017.10.026.

Homem CCF, Steinmann V, Burkard TR, Jais A, Esterbauer H, Knoblich JA (2014) Ecdysone and mediator change energy metabolism to terminate proliferation in drosophila neural stem cells. Cell 158:874–888 Available at: http://dx.doi.org/10.1016/j.cell.2014.06.024.

Huang DW, Sherman BT, Lempicki RA (2009a) Bioinformatics enrichment tools: Paths toward the comprehensive functional analysis of large gene lists. Nucleic Acids Res.

Huang DW, Sherman BT, Lempicki RA (2009b) Systematic and integrative analysis of large gene lists using DAVID bioinformatics resources. Nat Protoc.

Inagaki HK, Kamikouchi A, Ito K (2010) Methods for quantifying simple gravity sensing in Drosophila melanogaster. Nat Protoc 5:20–25 Available at: http://dx.doi.org/10.1038/nprot.2009.196.

Jenett A et al. (2012) A GAL4-Driver Line Resource for Drosophila Neurobiology. Cell Rep 2:991–1001 Available at: http://dx.doi.org/10.1016/j.celrep.2012.09.011.

Kanai MI, Kim MJ, Akiyama T, Takemura M, Wharton K, O'Connor MB, Nakato H (2018) Regulation of neuroblast proliferation by surface glia in the Drosophila larval brain. Sci Rep 8:1–15.

Koh YH, Popova E, Thomas U, Griffith LC, Budnik V (1999) Regulation of DLG localization at synapses by CaMKII-dependent phosphorylation. Cell.

Kushnir T, Mezuman S, Bar-Cohen S, Lange R, Paroush Z, Helman A (2017) Novel interplay between JNK and Egfr signaling in Drosophila dorsal closure. PLoS Genet 13:1–18.

Lanet E, Gould AP, Maurange C (2013) Protection of Neuronal Diversity at the Expense of Neuronal Numbers during Nutrient Restriction in the Drosophila Visual System. Cell Rep 3:587–594.

Lanet E, Maurange C (2014) Building a brain under nutritional restriction: Insights on sparing and plasticity from Drosophila studies. Front Physiol 5 MAR:1–9.

Layalle S, Arquier N, Léopold P (2008) The TOR Pathway Couples Nutrition and Developmental Timing in Drosophila. Dev Cell.

Li D, Liu Y, Pei C, Zhang P, Pan L, Xiao J, Meng S, Yuan Z, Bi X (2017) miR-285– Yki/Mask double-negative feedback loop mediates blood–brain barrier integrity in Drosophila. Proc Natl Acad Sci 114:E2365–E2374.

Marshall OJ, Brand AH (2015) Damidseq-pipeline: An automated pipeline for processing DamID sequencing datasets. Bioinformatics 31:3371–3373.

Marshall OJ, Southall TD, Cheetham SW, Brand AH (2016) Cell-type-specific profiling of protein – DNA interactions without cell isolation using targeted DamID with next-generation sequencing. Nat Protoc 11:1586–1598 Available at: http://dx.doi.org/10.1038/nprot.2016.084.

Mayer F, Mayer N, Chinn L, Pinsonneault RL, Kroetz D, Bainton RJ (2009) Evolutionary Conservation of Vertebrate Blood-Brain Barrier Chemoprotective Mechanisms in Drosophila. J Neurosci 29:3538–3550 Available at: http://www.jneurosci.org/cgi/doi/10.1523/JNEUROSCI.5564-08.2009.

Morin X, Daneman R, Zavortink M, Chia W (2001) A protein trap strategy to detect GFP-tagged proteins expressed from their endogenous loci in Drosophila. Proc Natl Acad Sci U S A 98:15050–15055.

Murugasu-Oei B, Rodrigues V, Yang X, Chia W (1995) Masquerade: A novel secreted serine protease-like molecule is required somatic muscle attachment in the Drosophila embryo. Genes Dev.

O'Brown NM, Pfau SJ, Gu C (2018) Bridging barriers: A comparative look at the blood-brain barrier across organisms. Genes Dev 32:466–478.

Øvrebø JI, Edgar BA (2018) Polyploidy in tissue homeostasis and regeneration. Development 145:dev156034.

Parkhurst SJ, Adhikari P, Navarrete JS, Legendre A, Manansala M, Wolf FW (2018) Perineurial Barrier Glia

Physically Respond to Alcohol in an Akap200-Dependent Manner to Promote Tolerance. Cell Rep 22:1647–1656.

Patrnogic J, Leclerc V (2017) The serine protease homolog spheroide is involved in sensing of pathogenic Gram-positive bacteria. PLoS One 12:1–13.

Pereanu W, Shy D, Hartenstein V (2005) Morphogenesis and proliferation of the larval brain glia in Drosophila. Dev Biol 283:191–203.

Prasad N, Hens K (2018) Sugar Promotes Feeding in Flies via the Serine Protease Homolog scarface. Cell Rep 24:3194-3206.e4 Available at: https://doi.org/10.1016/j.celrep.2018.08.059.

Rajan A, Perrimon N (2012) Drosophila cytokine unpaired 2 regulates physiological homeostasis by remotely controlling insulin secretion. Cell 151:123–137 Available at: http://dx.doi.org/10.1016/j.cell.2012.08.019.

Robinson JT, Thorvaldsdóttir H, Winckler W, Guttman M, Lander ES, Getz G, Mesirov JP (2011) Integrative genomics viewer. Nat Biotechnol.

Ross J, Jiang H, Kanost MR, Wang Y (2003) Serine proteases and their homologs in the Drosophila melanogaster genome: An initial analysis of sequence conservation and phylogenetic relationships. Gene 304:117–131.

Rousset R, Bono-Lauriol S, Gettings M, Suzanne M, Speder P, Noselli S (2010) The Drosophila serine protease homologue Scarface regulates JNK signalling in a negative-feedback loop during epithelial morphogenesis. Development 137:2177–2186.

Sandhu S, Kollah AP, Lewellyn L, Chan RF, Grotewiel M (2015) An inexpensive, scalable behavioral assay for measuring ethanol sedation sensitivity and rapid tolerance in Drosophila. J Vis Exp.

Schirmeier S, Klämbt C (2015) The Drosophila blood-brain barrier as interface between neurons and hemolymph. Mech Dev 138:50–55 Available at: http://dx.doi.org/10.1016/j.mod.2015.06.002.

Schwabe T, Bainton RJ, Fetter RD, Heberlein U, Gaul U (2005) GPCR signaling is required for blood-brain barrier formation in Drosophila. Cell 123:133–144.

Sorrosal G, Pérez L, Herranz H, Milán M (2010) Scarface, a secreted serine protease-like protein, regulates polarized localization of laminin A at the basement membrane of the Drosophila embryo. EMBO Rep 11:373–379.

Sousa-Nunes R, Yee LL, Gould AP (2011) Fat cells reactivate quiescent neuroblasts via TOR and glial insulin relays in Drosophila. Nature 471:508–513 Available at: http://dx.doi.org/10.1038/nature09867.

Southall TD, Gold KS, Egger B, Davidson CM, Caygill EE, Marshall OJ, Brand AH (2013) Cell-type-specific profiling of gene expression and chromatin binding without cell isolation: Assaying RNA pol II occupancy in neural stem cells. Dev Cell 26:101–112 Available at: http://dx.doi.org/10.1016/j.devcel.2013.05.020.

Spéder P, Brand AH (2014) Gap junction proteins in the blood-brain barrier control nutrient-dependent reactivation of Drosophila neural stem cells. Dev Cell 30:309–321.

Srivastava A, Dong Q (2015) Regulation of a serine protease homolog by the JNK pathway during thoracic development of Drosophila melanogaster. FEBS Open Bio 5:117–123 Available at: http://dx.doi.org/10.1016/j.fob.2015.01.008.

Stork T, Engelen D, Krudewig A, Silies M, Bainton RJ, Klambt C (2008) Organization and Function of the Blood Brain Barrier in Drosophila. J Neurosci 28:587–597 Available at: http://www.jneurosci.org/cgi/doi/10.1523/JNEUROSCI.4367-07.2008.

Sun H, Buchon N, Scott JG (2017) Mdr65 decreases toxicity of multiple insecticides in Drosophila melanogaster. Insect Biochem Mol Biol 89:11–16 Available at: https://doi.org/10.1016/j.ibmb.2017.08.002.

Szklarczyk D, Gable AL, Lyon D, Junge A, Wyder S, Huerta-Cepas J, Simonovic M, Doncheva NT, Morris JH, Bork P, Jensen LJ, Von Mering C (2019) STRING v11: Protein-protein association networks with increased coverage, supporting functional discovery in genome-wide experimental datasets. Nucleic Acids Res 47:D607–D613.

Tapadia MG, Lakhotia SC (2005) Expression of mdr49 and mdr65 multidrug resistance genes in larval tissues of Drosophila melanogaster under normal and stress conditions. Cell Stress Chaperones 10:7–11.

Uhlirova M, Bohmann D (2006) JNK- and Fos-regulated Mmp1 expression cooperates with Ras to induce invasive tumors in Drosophila. EMBO J 25:5294–5304.

Unhavaithaya Y, Orr-Weaver TL (2012) Polyploidization of glia in neural development links tissue growth to blood-brain barrier integrity. Genes Dev 26:31–36.

van den Ameele J, Brand AH (2019) Neural stem cell temporal patterning and brain tumour growth rely on oxidative phosphorylation. Elife 8:1–20 Available at: https://elifesciences.org/articles/47887 [Accessed September 30, 2019].

van den Ameele J, Krautz R, Brand AH (2019) TaDa! Analysing cell type-specific chromatin in vivo with Targeted DamID. Curr Opin Neurobiol 56:160–166 Available at: https://doi.org/10.1016/j.conb.2019.01.021.

Venken KJT, Schulze KL, Haelterman NA, Pan H, He Y, Evans-Holm M, Carlson JW, Levis RW, Spradling AC, Hoskins RA, Bellen HJ (2011) MiMIC: a highly versatile transposon insertion resource for engineering Drosophila melanogaster genes. Nat Methods 8:737–743 Available at: http://www.nature.com/articles/nmeth.1662.

Volkenhoff A, Weiler A, Letzel M, Stehling M, Klämbt C, Schirmeier S (2015) Glial glycolysis is essential for neuronal survival in drosophila. Cell Metab 22:437–447.

Von Stetina JR, Frawley LE, Unhavaithaya Y, Orr-Weaver TL (2018) Variant cell cycles regulated by Notch signaling control cell size and ensure a functional blood-brain barrier. Development 145:dev157115.

Wu JS, Luo L (2006) A protocol for dissecting Drosophila melanogaster brains for live imaging or immunostaining. Nat Protoc 1:2110–2115.

Yamada T, Habara O, Kubo H, Nishimura T (2018) Fat body glycogen serves as a metabolic safeguard for the maintenance of sugar levels in Drosophila. Development 145:dev158865 Available at: http://dev.biologists.org/lookup/doi/10.1242/dev.158865.

Yildirim K, Petri J, Kottmeier R, Klämbt C (2019) Drosophila glia: Few cell types and many conserved functions. Glia 67:5–26.

Zhang SL, Yue Z, Arnold DM, Artiushin G, Sehgal A (2018) A Circadian Clock in the Blood-Brain Barrier Regulates Xenobiotic Efflux. Cell 173:130-139.e10 Available at: https://doi.org/10.1016/j.cell.2018.02.017.

Zhao Z, Nelson AR, Betsholtz C, Zlokovic B V. (2015) Establishment and Dysfunction of the Blood-Brain Barrier. Cell 163:1064–1078 Available at: http://dx.doi.org/10.1016/j.cell.2015.10.067.

Zhu CC, Boone JQ, Jensen PA, Hanna S, Podemski L, Locke J, Doe CQ, O'Connor MB (2008) Drosophila Activin- and the Activin-like product Dawdle function redundantly to regulate proliferation in the larval brain. Development 135:513–521.

Figure Legends

Figure 1. Brain sparing as a model for understanding the adaptation to nutrient restriction. **(A)** Scheme showing our nutrient restriction (NR) protocol for Targeted DamID (TaDa) experiments. **(B-D)** Larval brains stained for DNA (green) at **(B)** 6 days after larval hatching (ALH), **(C)** 7 days ALH in Fed conditions and **(D)** 7 days ALH in NR conditions. Scale bar is 100 µm. **(E)** Quantification of brain volume. "n" is 20, 13 and 16 brains. One-way ANOVA and Tukey's multiple comparisons test were performed. **(F-G)** Comparison of pupal size on **(F)** Fed or **(G)** NR. Scale bar is 1 mm. **(H)** Graph showing the pupal volume in Fed and NR animals. "n" is 55 and 52 pupae respectively. Mann Whitney test was performed. **(I-L)** Representative **(I, K)** male and **(J, L)** female adult flies in **(I, J)** Fed or **(K, L)** NR conditions. **(M, N)** Immunostaining against Fas2 (green), CadN (red) and DNA (blue) of adult brains of animals in **(M)** Fed or **(N)** NR conditions during larval development. Scale bar is 100 µm. **(O)** Plot showing the area of adult brains after Fed or NR protocol. "n" is 12 adult brains for each conditions. Unpaired Student's T-test was used **** is p-value < 0.0001.

Figure 2. Targeted DamID in neuroblasts and glial cells of the blood-brain barrier after nutrient restriction. (A) Schematic representation of the different cell types in the larval brain. BBB, blood-brain barrier; CG, cortex glia; GMC, ganglion mother cells; N, neuron; NB, neuroblast; NG, neuropil glia; PG, perineurial glia; SPG, subperineurial glia. See Figure 2-1 for a schematic representation. **(B-B'')** Confocal images of larval brain expressing mCD8-GFP in Superficial Glia (PG and SPG, *sema5c-GAL4, UAS-mCD8-GFP,* green and grey) and mtdTomato

in SPG *(mdr65-mtdTomato,* red and grey). Arrowheads show the overlap of the green and red signals. Scale bar is 20 µm. PolII binding in BBB marker genes can be found in Figure 2-1 **(C)** Heatmap diagram showing correlation of all Fed and NR TaDa libraries. **(D-F)** Volcano plots showing PolII bound genes in NR and Fed conditions in **(D)** neuroblasts (NB), **(E)** subperineurial (SPG) and **(F)** surface glia (SG, SPG+PG). Genes differentially bound by PolII between Fed and NR conditions are highlighted in red. **(G)** Graph showing the Gene Ontology (GO) categories enriched in genes downregulated in NBs by NR. Check Figure 2-1. **(H-J)** Heatmaps showing the PolII binding of differentially expressed genes in the TaDa replicates of **(H)** NBs, **(I)** SPG and **(J)** SG. Tables of PolII binding in all genes are in Figure 2-2.

Figure 3. Nutrient restriction does not affect neuroblast proliferation and pathway activation in the BBB. (A) Neuroblast (NB) diameter during mitosis (green dots) and interphase (magenta dots) of w^{1118} larval brains in Fed and NR conditions. "n" is 9 and 7 brain lobes respectively. Two-way ANOVA and Bonferroni's multiple comparisons test were performed. **(B)** Graph showing the NB mitotic index of w^{1118} larval brains under Fed and NR conditions. "n" is 10 and 8 brain lobes respectively. Unpaired Student's T-test was performed. ns is non-significant. **(C, D)** Larval central nervous systems immunostained for CadN (neuropil marker in green) and DNA (red) under **(C)** Fed or **(D)** NR conditions. **(E)** Plot showing the quantification of the relative size of the neuropil (neuropil/whole brain) from **(C, D)**. "n" is 13 and 12 CNS respectively. Unpaired Student's T-test was performed, **** is p-value <0.0001. **(F-I')** Ventral nerve cords of **(F-G')** JAK-STAT (*10xSTAT92E-GFP*) and **(H-I')** JNK (*TRE-RFP*) pathway reporters under **(F, F', H, H')** Fed and **(G, G', I, I')** NR conditions. **(F-G')** Immunofluorescences for GFP (green and grey), Repo (red)

and Elav (blue). **(H-I')** Immunofluorescences for Repo (green) and RFP (red and grey). Scale bars are 20 µm.

Figure 4. Nutrient restriction affects the growth of the blood-brain barrier. (A-D) Analysis of larval subperineurial glia (SPG) endomitosis of animals (*mdr65-GAL4, UAS-DlgA::GFP*) in Fed and NR conditions. **(A)** Graph showing the average number of SPG nuclei per brain lobe. "n" is 49 and 47 brain lobes. Unpaired Student's T-test was performed. **(B)** Plot showing the percentage of multinucleated SPG (2 or more nuclei) per brain lobe. "n" is 48 and 47 brain lobes respectively. Mann Whitney test was done. **(C)** Plot showing the number of nuclei in each SPG analysed, median (black line) and interquartile range are shown. Mann Whitney test was done, Fed and NR "n" is 242 and 313 SPG respectively. **(D)** Histogram depicting the relative distribution (percentage) of SPG according to the number of nuclei. **(E)** Graph showing the average size of the SPG nucleus (*moody-GAL4, UAS-GFP.nls*) of larval brains in Fed and NR conditions. "n" is 24 and 23 brain lobes respectively. Unpaired Student's T-test was used is p-value. **(F)** Plot showing the distribution of the number of perineurial glia (PG) per brain lobe. *moody-GAL4, UAS-GFP.nls* were stained for the glial marker Repo and PG were scored as Repo-positive/GFP-negative nuclei. "n" is 26 brain lobes for Fed and NR conditions. Unpaired Student's T-test was used. **(G, H)** Larval brain lobes of *lac::GFP* animals under **(G)** Fed and **(H)** NR conditions, showing the integrity of septate junctions. Scale bars are 50 µm. **(I, J)** Blood-brain barrier permeability assay in *mdr65-GAL4, UAS-mCD8-GFP* animals under **(I)** Fed or **(J)** NR conditions. Images show the ventral nerve cord, SPG membrane in green and 10 kDa Dextran-Rhodamine in red. Plots show the intensity of fluorophores across the yellow line in each image. Scale bar is 20 µm. **, *** and **** are p-value <0.01, <0.001 and < 0.0001 respectively.

Figure 5. Scarface is a nutrient sensitive gene expressed in the *Drosophila* blood-brain barrier. (A) Genome view of the *scaf* locus and the binding of PolII in SPG TaDa in Fed (blue) and NR (red) conditions. Note the reduction on PolII binding in NR compared to Fed. **(B-C'')** Immunostaining of *scaf::GFP* (*scaf*^{PBss}, in green) larval brain lobes (optical section at the BBB level) under **(B-B'')** Fed and **(C-C'')** NR conditions stained for Repo (glial marker in red). **(B'', C'')** are colour-coded images of Scaf::GFP signal. (D-E'') Immunostaining of larval brains under **(D-D'')** Fed and **(E-E'')** NR conditions stained for Scaf (green) and Repo (red). **(D'', E'')** are colour-coded images of anti-Scaf antibody signal. **(F, G)** Graph showing the quantification of the Scaf signal in the BBB using **(F)** Scaf::GFP reporter ("n" is 7 and 8 brains) or **(G)** anti-Scaf antibody ("n" is 11 brains). Unpaired Student's T-test was used, *** is p-value < 0.001. **(H)** Confocal images of a larval brain stained with anti-Scaf (green) and Dpn (NB marker in red). **(I, I')** Larval brain expressing mCD8GFP in SPG (*mdr65-Gal4, UASmCD8-GFP*, in red) and stained for Repo (glial marker in blue) and Scaf (green or grey). **(J-J'')** Cross section of larval BBB of *mdr65-GAL4, UAS-mCD8GFP* animals stained against Repo (blue), Scaf (green or grey) and mCD8-GFP (red or grey). **(K-K'')** 3D reconstruction of the larval BBB of *mdr65-GAL4, UAS-mCD8GFP* animals stained against Repo (blue), Scaf (green) and mCD8-GFP (red). **(L-L'')** Representative confocal image of a cross section of a larval brain stained against Scaf (blue and grey), *sema5-GAL4, UAS-mCD8-RFP* (red) and LanA::GFP (green and grey) as a neural lamella marker. Scale bars are 20 µm for (B-E'', H-J'') and 10 µm for (L-L''). **(M)** Graphic representation of the regulation of *scaf* expression in the blood-brain barrier by nutrition.

Figure 6. Scarface is necessary for controlling the growth of the blood-brain barrier. (A-C') Immunostaining of larval brains of *mdr65-GAL4, UAS-mCD8GFP* animals crossed to **(A, A')** w^{1118} (control), **(B, B')** *UAS-shScaf*^{RNAi} and **(C, C')** *UAS-lhScaf*^{RNAi}, and stained for Repo (blue), Scaf (red and grey) and GFP (green). Scale bars are 50 µm. **(D)** Plot showing the quantification of *scaf* knockdown. "n" is 6, 7, 6 brains respectively. One-way ANOVA and Dunnett's multiple comparisons test were performed. **(E, F)** Images of pupae of *mdr65-GAL4* crossed to **(E)** w^{1118} (control) and **(F)** *UAS-shScaf*^{RNAi}. **(G)** Plot showing the pupal volume for each group. "n" are 45 and 52 pupae respectively. Mann-Whitney test was performed. **(H)** Graph showing the timing of pupariation of *mdr65-GAL4* crossed to w^{1118} (Ctrl, dark) or *UAS-shScaf*^{RNAi} (red). "n" is 6 groups of about 35-40 larvae for each condition. **(I, J)** Larval central nervous system of *mdr65-GAL4, UAS-DlgA:EGFP* animals crossed to **(I)** w^{1118} (control) and **(J)** *UAS-shScaf*^{RNAi}. *UAS-DlgA:EGFP* labels SPG nuclei and septate junction. Scale bars are 100 µm. *scaf* knockdown and over-expression effect over animal development is shown in Figure 5-1. **(K-N)** Analysis of larval subperineurial glia (SPG) endomitosis. *mdr65-GAL4, UAS-DlgA::GFP* animals were crossed to w^{1118} (control) and *scaf* knockdown (*UAS-shScaf*^{RNAi}). **(K)** Graph showing the average number of SPG nuclei per brain lobe. "n" is 43 and 46 brain lobes. Unpaired Student's T-test was performed. **(L)** Plot showing the percentage of multinucleated SPG (2 or more nuclei) per brain lobe. "n" is 43 and 56 brain lobes. Mann Whitney test was done. **(M)** Plot showing the number of nuclei in each SPG analysed, median (black line) and interquartile range are shown. Mann Whitney test was done, "n" is 230 (Ctrl) 320 (shScaf^{RNAi}) SPG. **(N)** Histogram showing the relative distribution (percentage) of SPG according to the number of nuclei. **(O)** Graph showing the average size of the SPG nucleus of larval brains. *mdr65-GAL4, UAS-DlgA::GFP* animals were crossed to w^{1118} (control) and *UAS-shScaf*^{RNAi}. "n" is 44 and 56 brain lobes respectively. Unpaired Student's T-test

was used. **(P)** Plot showing the distribution of the number of perineurial glia (PG) per brain lobe. *mdr65-GAL4, UAS- DlgA::GFP* were stained for the glial marker Repo, Repo-positive/GFP-negative nuclei were counted as PG. "n" is 26 brains for both condition. Unpaired Student's T-test was performed. **(Q, R)** Blood-brain barrier permeability assay in *mdr65-GAL4, UAS-mCD8-GFP* animals crossed to **(Q)** w^{1118} (control) or **(R)** *UAS-shScaf*^{RNAi}. Images show the ventral nerve cord, SPG membrane in green and 10 kDa Dextran-Rhodamine in red. *, **, *** and **** are p-value <0.05, <0.01, <0.001 and <0.0001 respectively. ns is non-significant. *scaf* knockdown using UAS-lh*Scaf*^{RNAi} is shown in Figure 6-1.

Figure 7. Scarface overexpression in subperineurial glia affects larval development and the growth of the BBB. **(A-D)** Images of pupae of *mdr65-GAL4* crossed to **(A, C)** w^{1118} or **(B, D)** *UAS-Scaf::GFP* (Scaf OE) under **(A, B)** Fed or **(C, D)** NR conditions. Scale bar is 1 mm. **(E)** Graph showing the pupal volume. "n" is 57, 57, 67 and 70 pupae respectively. Two-way ANOVA and Bonferroni's multiple comparisons tests were done. **(F)** Graph showing the timing of pupariation of *mdr65-GAL4* crossed to w^{1118} (Ctrl, dark) or *UAS-Scaf::GFP* (Scaf OE, green). "n" is 6 groups of around 35-40 larvae for each condition. **(G-J)** Analysis of larval subperineurial glia (SPG) endomitosis of *mdr65-GAL4, UAS-DlgA::GFP* animals crossed to w^{1118} (control) and *UAS-Scaf::GFP* (Scaf OE). **(G)** Graph showing the average number of SPG nuclei per brain lobe. "n" is 88 and 84 brain lobes. Unpaired Student's T-test was performed. **(H)** Plot showing the percentage of multinucleated SPG (2 or more nuclei) per brain lobe. "n" is 89 and 84 brain lobes. Mann Whitney test was done. **(I)** Histogram showing the relative distribution (percentage) of SPG according to the number of nuclei. **(J)** Plot showing the number of nuclei in each SPG analysed, median (black bar) and interquartile range are shown. Mann Whitney test was done, "n" is 531

(Ctrl) and 440 (Scaf OE) SPG. **(K)** Plot showing of the average size of SPG nuclei. *moody-GAL4, UAS-GFP.nls* was crossed to w^{1118} (control) and *UAS-Scaf::GFP* (Scaf OE). "n" is 26 brain lobes for each condition. Unpaired Student's T-test was used. **(L)** Plot showing the distribution of the number of perineurial glia (PG) in brain lobe. *moody-GAL4, UAS-GFP.nls* were stained for the glial marker Repo, Repo-positive/GFP-negative nuclei were scored as PG. "n" is 26 and 24 brain lobes. Unpaired Student's T-test was used. *, **, *** and **** are p-value <0.05, <0.01, <0.001 and <0.0001 respectively. ns is non-significant.

Figure 8. Scarface modulates neurogenesis in the larval brain. (A, B) Immunostaining of larval brains of *mdr65-GAL4* crossed to **(A)** w^{1118} (control) and **(B)** *UAS-shScaf*^{RNAi}, stained for the NB marker Dpn (red) and phospho-Histone H3 (pH3 in green). Scale bar is 20 µm. **(C)** Graph showing the NB mitotic index (percentage of pH3-positive NB) of control and *scaf* knockdown brains. "n" is 34 and 35 brain lobes respectively. Unpaired Student's T-test was performed. **(D)** Graph showing the NB mitotic index of *scaf*$^{27/+}$ (heterozygous) and *scaf*$^{27/MI09409}$, "n" is 12 and 11 brain lobes respectively. Unpaired Student's T-test was performed. **(E)** NB mitotic index of *scaf*$^{PBss/+}$, *mdr65-GAL4* (heterozygous); *scaf*$^{PBss/27}$, *mdr65-GAL4*; and *scaf*$^{PBss/27}$; *mdr65-GAL4, UAS-Scaf:GFP* animals. "n" is 26, 27 and 27 brain lobes respectively. One-way ANOVA and Dunnett's multiple comparisons test were performed. **(F)** Plot of the size of the adult brain of *mdr65-GAL4* crossed to w^{1118} (control) and *UAS-shScaf*^{RNAi}. "n" is 39 and 41 adult brains respectively. Unpaired Student's T-test was performed. * and **** are p-value <0.05 and <0.0001 respectively. ns is non-significant. **(G)** Working model of Scaf function in the *Drosophila* blood-brain barrier. As a response to nutrient availability, the subperineurial glial cells in the BBB express Scaf. Scaf slows

down the growth of SPG and diminishes the proliferation of PG, but at the same time promotes NB proliferation.

Figure 9. Expression of Scarface in subperineurial glia increases neurogenesis during nutrient restriction. (A, B) Adult brains stained for CadN (green) of *mdr65-GAL4* crossed to **(A)** w^{1118} (control) and **(B)** *UAS-Scaf::GFP* (Scaf OE) under nutrient restriction (NR). Scale bar is 100 µm. **(C)** Quantification of the adult brain area. *mdr65-GAL4* animals were crossed to w^{1118} (control) and *UAS-Scaf::GFP* (Scaf OE) under NR. "n" is 38 and 37 adult brains respectively. Unpaired Student's T-test was performed. **(D)** Graph of the NB mitotic index of *mdr65-GAL4* animals crossed to w^{1118} (control) and *UAS-Scaf::GFP* (Scaf OE) larval brains under NR. "n" is 11 and 13 brain lobes respectively. Unpaired Student's T-test was performed. **(E-H)** Analysis of larval subperineurial glia (SPG) endomitosis of *mdr65-GAL4, UAS-DlgA::GFP* animals crossed to w^{1118} (control) and *scaf* overexpression (*UAS-Scaf::GFP*, Scaf OE) under nutrient restriction (NR). **(E)** Graph showing the average number of SPG nuclei per brain lobe. "n" is 28 and 26 brain lobes. Unpaired Student's T-test was performed. **(F)** Plot showing the percentage of multinucleated SPG (2 or more nuclei) per brain lobe. "n" is 28 and 26 brain lobes. Mann Whitney test was used. **(G)** Plot showing the number of nuclei in each SPG analysed, median (black line) and interquartile range are shown. Mann Whitney test was performed, "n" is 182 (Ctrl) and 183 (Scaf OE) SPG. **(H)** Histogram depicting the relative distribution (percentage) of SPG according to the number of nuclei. **(I)** Graph showing the average size of the SPG nucleus of larval brains of *moody-GAL4, UAS-GFP.nls* animals crossed to w^{1118} (control) and Scaf overexpression (*UAS-Scaf::GFP*, Scaf OE) under NR. "n" is 30 and 26 brain lobes. Unpaired Student's T-test was used. **(J)** Plot showing the distribution of the number of perineurial glia (PG) per brain lobe. *moody-*

GAL4, UAS-GFP.nls were crossed to w^{1118} (control) and Scaf overexpression (*UAS-Scaf::GFP*, Scaf OE) under NR, and stained for the glial marker Repo. Repo-positive/GFP-negative nuclei were scored as PG. "n" is 30 and 26 brain lobes. Unpaired Student's T-test was used. **(K, L)** Immunostaining against CadN of adult female brains of *mdr65-GAL4* crossed to **(K)** w^{1118} (Ctrl) or **(L)** *UAS-Scaf::GFP* (Scaf OE). Scale bar is 100 µm. **(M)** Plot showing the size of the adult brain of *mdr65-GAL4* crossed to w^{1118} (control) and *UAS-Scaf::GFP* (Scaf OE). "n" is 16 and 13 adult brains respectively. Unpaired Student's T-test was performed. **(N-Q)** Wings of male animals of *mdr65-GAL4* crossed to **(N, O)** w^{1118} (Ctrl) and **(P, Q)** *UAS-Scaf::GFP* (Scaf OE) under **(N, P)** Fed or **(O, Q)** NR conditions. Scale bar is 1 mm. **(R)** Plot showing the quantification of the size of the wings for each conditions. "n" is 29, 30, 30 and 30 wings respectively. Two-way ANOVA and Tukey multiple comparison tests were done. *, **** and ns are p-value <0.05, <0.0001 and non-significant respectively.

Figure 10. Locomotion activity is not altered upon *scaf* knockdown in the blood-brain barrier. (A-C) Locomotion assays of *mdr65-GAL4* animals crossed to w^{1118} (control) and $shScaf^{RNAi}$. Graphs showing the larval **(A)** average and **(B)** maximum speed. "n" is 67 and 65 larvae. **(C)** Plot of the adult climbing index using a Countercurrent apparatus. "n" is 8 groups of about 25 adult flies for each genotype. Unpaired Student's T-test were performed. **(D)** Activity measurements using the DAM2 system. Plot shows the daily number of counts per day of single adult flies of w^{1118} crossed to *UAS-shScaf*^{RNAi} (dark dots, control), *mdr65-GAL4* crossed to w^{1118} (open dots, control) and *mdr65-GAL4* crossed to *UAS-shScaf*^{RNAi} (red dots). "n" is 30, 32 and 30 adult flies respectively. One-way ANOVA and Dunnett's multiple comparisons test were performed. **(E)** Sleep assay using the DAM2 system. Graph showing the average sleep fraction

per day of single adult flies of the genotypes: w^{1118} crossed to *UAS-shScaf*^{RNAi} (dark dots, control), *mdr65-GAL4* crossed to w^{1118} (open dots, control) and *mdr65-GAL4* crossed to *UAS-shScaf*^{RNAi} (red dots). "n" is 30, 32 and 30 adult flies respectively. One-way ANOVA and Dunnett's multiple comparisons test were performed. **(F)** Activity and **(G)** sleep profiles showing average values in each time point in a 12:12 light:dark cycle. Adult flies of the genotypes: w^{1118} crossed to *UAS-shScaf*^{RNAi} (dark dots, control), *mdr65-GAL4* crossed to w^{1118} (open dots, control) and *mdr65-GAL4* crossed to *UAS-shScaf*^{RNAi} (red dots). "n" is 30, 32 and 30 adult flies respectively. ZT is Zeitgeber time. ns means non-significant.

Figure 11. Drug sensitivity is affected by *scaf* knockdown in the blood-brain barrier. (A, B) Ethanol sensitivity assay. **(A)** Graph showing the inactive fraction of flies at different time points. Adult flies of *mdr65-GAL4* animals crossed to w^{1118} (control, dark dots) and *UAS-shScaf*^{RNAi} (*scaf* knockdown, red dots). **(B)** Sedation time 50 (ST50) was calculated from **(A)**. **(B)** Bar chart showing ST50 for each genotype. "n" is 5 groups of 8-10 adult flies for each genotype. Unpaired Student's T-test was performed. **(C)** Insecticide resistance assay. Adult flies of *mdr65-GAL4* crossed to w^{1118} (control, dark dots), *UAS-shScaf*^{RNAi} (*scaf* knockdown, red dots) and *UAS-lhScaf*^{RNAi} (*scaf* knockdown, cyan dots). Plot shows the lethal fraction after 12, 24 and 36 hrs of exposure to 0.01% malathion. "n" is 4 groups of 20 adult flies for each genotype. Two-way ANOVA and Dunnett's multiple comparisons test were done. **(D, E)** Ethanol sensitivity assay of male w^{1118} flies that grew under Fed or NR conditions. **(D)** Graph showing the inactive fraction of flies at different time points. Fed (blue) and NR (red). **(E)** Sedation time 50 (ST50) was calculated from **(D)**. **(E)** Bar chart showing ST50 for Fed and NR conditions. "n" is 8 and 6 groups of 8 adult flies each. Unpaired Student's T-test was performed. ** and **** are p-value <0.01 and <0.0001

respectively. **(F, G)** Expression of the *mdr65-GAL4* driver in adult tissues. **(F)** Images of the adult brain and **(G)** hindgut (arrowhead) and malpighian tubules (arrow). DAPI was used to stain DNA (blue) and *UAS-lam:GFP* (green) for marking nuclei. **(H, I)** Blood-brain barrier permeability assay in *mdr65-GAL4* animals crossed to **(H)** w^{1118} (control) or **(I)** *UAS-shScaf*^{RNAi}. Images show adult brains, DNA was stained with DAPI in blue and 10 kDa Dextran-Rhodamine in red. Scale bars are 100 µm.

Extended Data legends

Figure 2-1. (A) Drivers used for TaDa in different cell populations. **(B)** Scheme of the TaDa mechanism showing the binding of the NDam-PolII fusion protein to the DNA and the methylation in GATC sequence. **(C)** Meta-analysis of the NDam-PolII binding using the driver *wor-GAL4* (NSC, neuroblast). Graph shows NDam-PolII in Fed and NR replicates. **(D-G)** Genome view of the **(D)** *moody*, **(E)** *mdr65*, **(F)** *Tret1-1* and **(G)** *vkg* and *Col4a1* loci, showing the binding of PolII using *sema5c-GAL4* (blue track) and *mdr65-GAL4* (green track) drivers under normal Fed conditions. Note that the binding of PolII across *moody* and *mdr65*, markers of subperineurial glia, is similar in both drivers, however, the perineurial markers *Tret1-1*, *vkg* and *Col4g1* are only bound by PolII in *sema5c-GAL4* dataset. **(H, I)** Diagram showing a String association network of genes downregulated in **(H)** NBs and **(I)** Subperineurial glia during NR. Genes associated to the JNK pathway are shown surrounded by a grey background in **(I)**.

Figure 2-2. Tables of genes differentially bound by PolII during Fed and NR conditions in NB, SPG and SG TaDa. PolII binding and FDR are given for average data in Fed and NR conditions. The difference of PolII binding between Fed and NR (diff) and the ratio between them are shown.

Figure 6-1. (A-D) Analysis of larval subperineurial glia (SPG) endomitosis of *mdr65-GAL4, UAS-DlgA::GFP* animals crossed to w^{1118} (control) and *UAS-lhScaf*^{RNAi} (*scaf* knockdown). **(A)** Graph showing the average number of SPG nuclei per brain lobe. "n" is 60 and 37 brain lobes. Unpaired Student's T-test was performed. **(B)** Plot showing the percentage of multinucleated SPG (2 or more nuclei) per brain lobe. "n" is 60 and 37 brain lobes. Mann Whitney test was done. **(C)** Plot showing the number of nuclei in each SPG analysed, median (black line) and interquartile range are shown. Mann Whitney test was done, "n" is 374 and 189 SPG for Ctrl and lhScaf^{RNAi} respectively. **(D)** Histogram depicting the relative distribution (percentage) of SPG according to the number of nuclei. **(E)** Graph showing the average size of the SPG nucleus of larval brains of *mdr-GAL4, UAS-DlgA::GFP* animals crossed to w^{1118} (control) and *UAS-lhScaf*^{RNAi}. "n" is 30 and 27 brain lobes respectively. Unpaired Student's T-test was used. **(F)** Plot showing the distribution of the number of perineurial glia (PG) per brain lobe. *mdr65-GAL4, UAS-GFP.nls* were crossed to w^{1118} (control) and *UAS-lhScaf*^{RNAi} and stained for the glial marker Repo. Repo-positive/GFP-negative nuclei were scored as PG. "n" is 24 and 26 brain lobes. Unpaired Student's T-test was used. *, **, *** and **** are p-value <0.05, <0.01, <0.001 and < 0.0001 respectively.

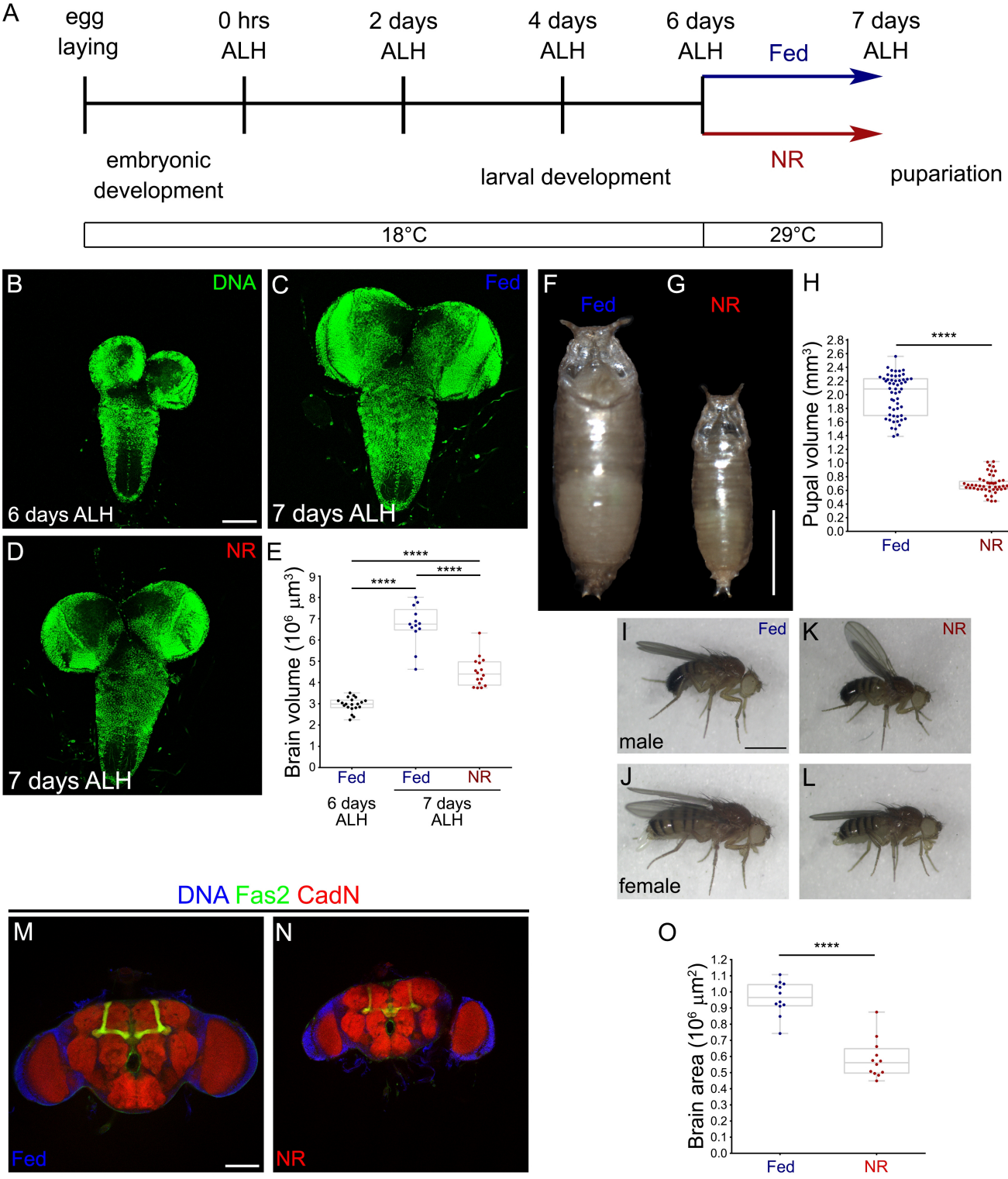
A
egg laying
0 hrs ALH
2 days ALH
4 days ALH
6 days ALH
Fed
7 days ALH
NR
embryonic development
larval development
pupariation
18°C
29°C
B
DNA
6 days ALH
C
Fed
7 days ALH
D
NR
7 days ALH
E
Brain volume (10^6 µm^3)
****
****
****
Fed
Fed
NR
6 days ALH
7 days ALH
F
Fed
G
NR
H
Pupal volume (mm^3)
****
Fed
NR
I
Fed
male
K
NR
J
female
L
DNA Fas2 CadN
M
Fed
N
NR
O
Brain area (10^6 µm^2)
****
Fed
NR

Figure 1

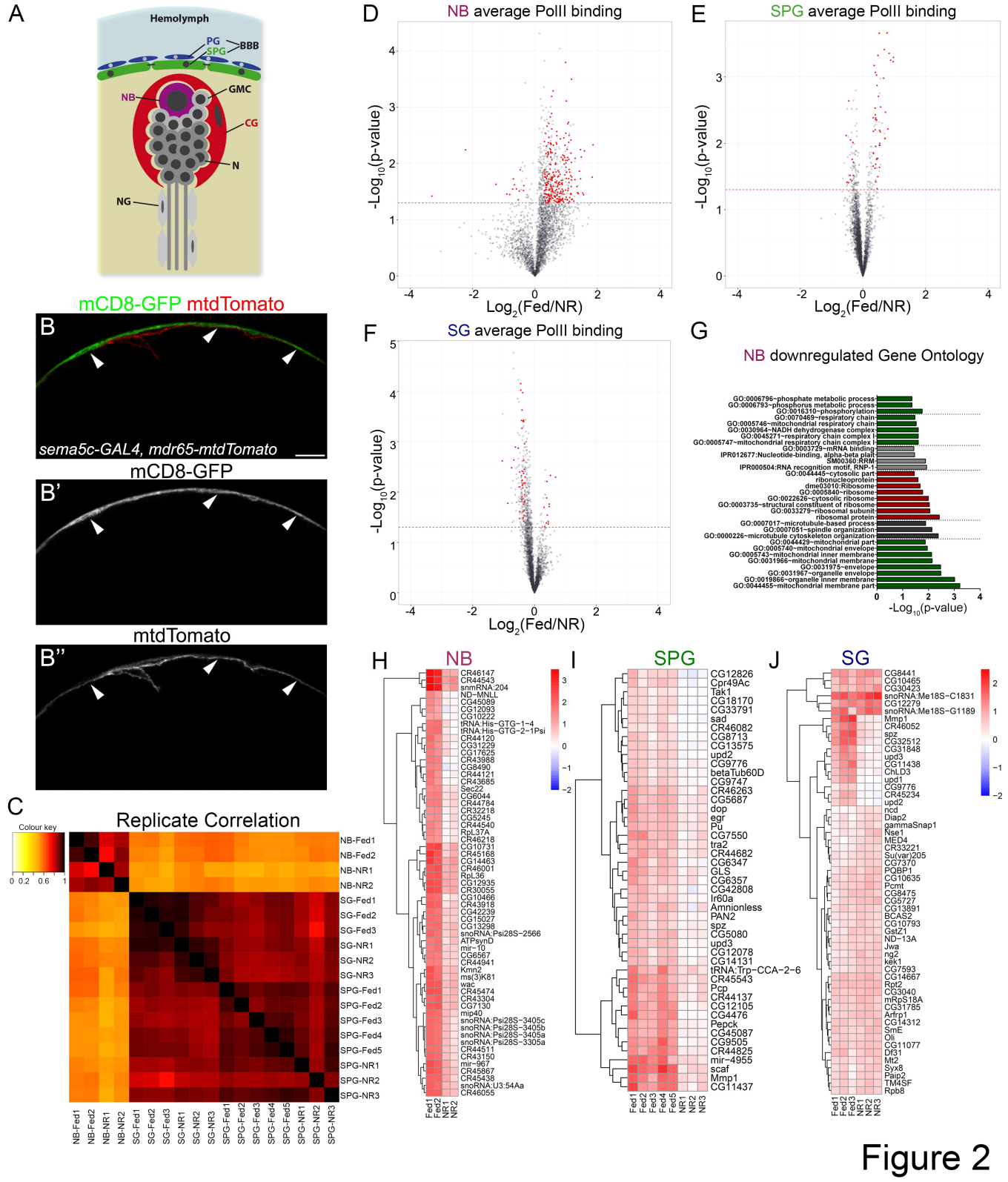
A
Hemolymph
PG
SPG
BBB
NB
GMC
CG
N
NG
mCD8-GFP mtdTomato
B
sema5c-GAL4, mdr65-mtdTomato
mCD8-GFP
B'
mtdTomato
B''
C
Replicate Correlation
Colour key
0 0.2 0.6 1
NB-Fed1
NB-Fed2
NB-NR1
NB-NR2
SG-Fed1
SG-Fed2
SG-Fed3
SG-NR1
SG-NR2
SG-NR3
SPG-Fed1
SPG-Fed2
SPG-Fed3
SPG-Fed4
SPG-Fed5
SPG-NR1
SPG-NR2
SPG-NR3
D
NB average PolII binding
-Log10(p-value)
Log2(Fed/NR)
E
SPG average PolII binding
-Log10(p-value)
Log2(Fed/NR)
F
SG average PolII binding
-Log10(p-value)
Log2(Fed/NR)
G
NB downregulated Gene Ontology
GO:0006796~phosphate metabolic process
GO:0006793~phosphorus metabolic process
GO:0016310~phosphorylation
GO:0070469~respiratory chain
GO:0005746~mitochondrial respiratory chain
GO:0030964~NADH dehydrogenase complex
GO:0045271~respiratory chain complex I
GO:0005747~mitochondrial respiratory chain complex I
GO:0003729~mRNA binding
IPR012677:Nucleotide-binding, alpha-beta plait
SM00360:RRM
IPR000504:RNA recognition motif, RNP-1
GO:0044445~cytosolic part
ribonucleoprotein
dme03010:Ribosome
GO:0005840~ribosome
GO:0022626~cytosolic ribosome
GO:0003735~structural constituent of ribosome
GO:0033279~ribosomal subunit
ribosomal protein
GO:0007017~microtubule-based process
GO:0007051~spindle organization
GO:0000226~microtubule cytoskeleton organization
GO:0044429~mitochondrial part
GO:0005740~mitochondrial envelope
GO:0005743~mitochondrial inner membrane
GO:0031966~mitochondrial membrane
GO:0031975~envelope
GO:0031967~organelle envelope
GO:0019866~organelle inner membrane
GO:0044455~mitochondrial membrane part
-Log10(p-value)
H
NB
CR46147
CR44543
snmRNA:204
ND-MNLL
CG45089
CG12093
CG10222
tRNA:His-GTG-1-4
tRNA:His-GTG-2-1Psi
CR44120
CG31229
CG17625
CR43988
CG8490
CR44121
CR43685
Sec22
CG6044
CR44784
CR32218
CG5245
CR44540
RpL37A
CR46218
CG10731
CR45168
CR44463
CR46001
RpL36
CG12935
CR30055
CG10466
CR43918
CG42239
CG15027
CG13298
snoRNA:Psi28S-2566
ATPsynD
mir-10
CG6567
CR44941
Kmn2
ms(3)K81
wac
CR45474
CR43304
CG7130
mip40
snoRNA:Psi28S-3405c
snoRNA:Psi28S-3405b
snoRNA:Psi28S-3405a
snoRNA:Psi28S-3305a
CR44511
CR43150
mir-967
CR45867
CR45438
snoRNA:U3:54Aa
CR46055
Fed1
Fed2
Fed3
NR1
NR2
I
SPG
CG12826
Cpr49Ac
Tak1
CG18170
CG33791
sad
CR46082
CG8713
CG13575
upd2
CG9776
betaTub60D
CG9747
CR46263
CG5687
dop
egr
Pu
CG7550
tra2
CR44682
CG6347
GLS
CG6357
CG42808
Ir60a
Amnionless
PAN2
spz
CG5080
upd3
CG12078
CG14131
tRNA:Trp-CCA-2-6
CR45543
Pcp
CR44137
CG12105
CG4476
Pepck
CG45087
CG9505
CR44825
mir-4955
scaf
Mmp1
CG11437
Fed1
Fed2
Fed3
Fed4
Fed5
NR1
NR2
NR3
J
SG
CG8441
CG10465
CG30423
snoRNA:Me18S-C1831
CG12279
snoRNA:Me18S-G1189
Mmp1
CR46052
spz
CG32512
CG31848
upd3
CG11438
ChLD3
upd1
CG9776
CR45234
upd2
ncd
Diap2
gammaSnap1
Nse1
MED4
CR33221
Su(var)205
CG7370
PQBP1
CG10635
Pcmt
CG8475
CG5727
CG13891
BCAS2
CG10793
GstZ1
ND-13A
Jwa
ng2
kek1
CG7593
CG14667
Rpt2
CG3040
mRpS18A
CG31785
Arfrp1
CG14312
SmE
Obi
CG11077
Dfd31
Mt2
Syx8
Paip2
TM4SF
Rpb8
Fed1
Fed2
Fed3
NR1
NR2
NR3

Figure 2

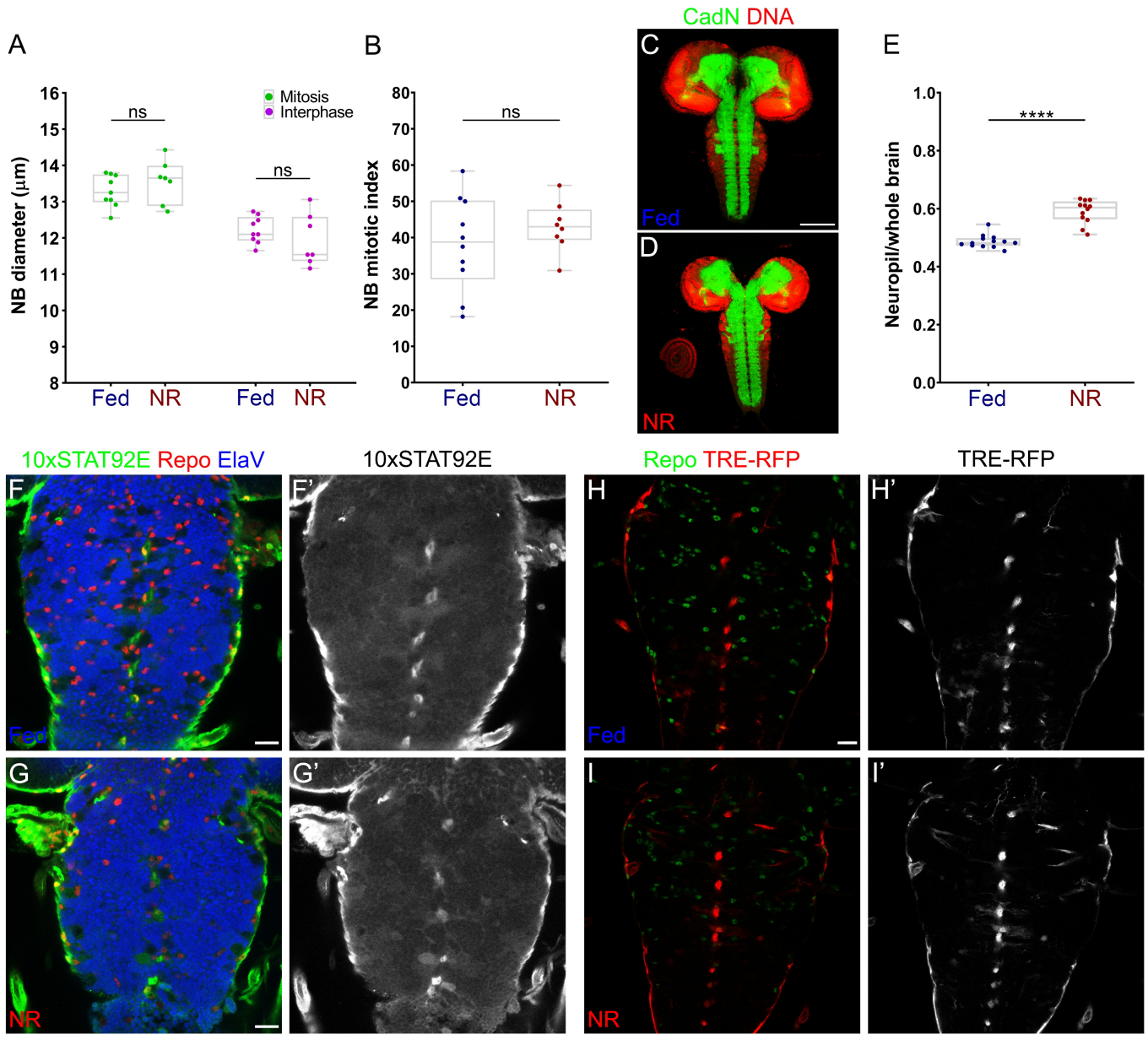
A
NB diameter (µm)
16
15
14
13
12
11
10
9
8
ns
ns
Mitosis
Interphase
Fed
NR
Fed
NR
B
NB mitotic index
80
70
60
50
40
30
20
10
0
ns
Fed
NR
CadN DNA
C
Fed
D
NR
E
Neuropil/whole brain
1.0
0.8
0.6
0.4
0.2
0.0
****
Fed
NR
10xSTAT92E Repo ElaV
10xSTAT92E
F
F'
Fed
G
G'
NR
Repo TRE-RFP
TRE-RFP
H
H'
Fed
I
I'
NR

Figure 3

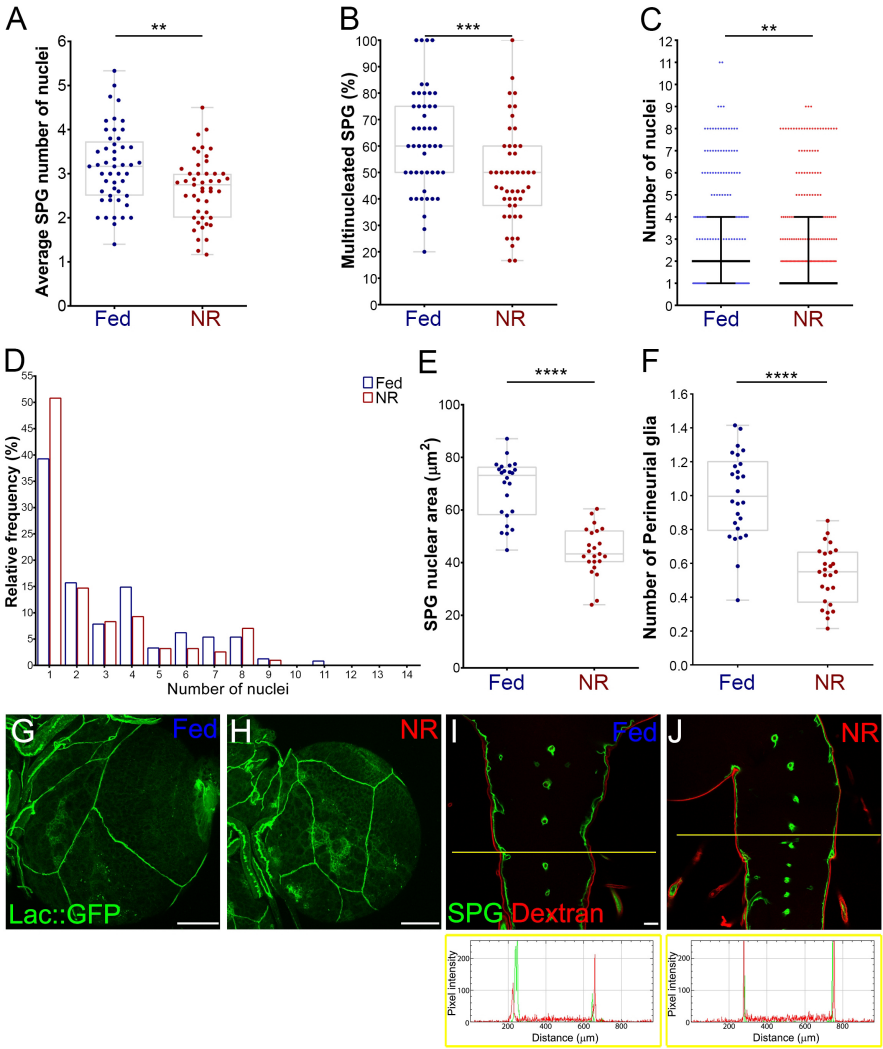
A
Average SPG number of nuclei
**
Fed
NR
B
Multinucleated SPG (%)
***
Fed
NR
C
Number of nuclei
**
Fed
NR
D
Fed
NR
Relative frequency (%)
Number of nuclei
E
SPG nuclear area (μm²)
****
Fed
NR
F
Number of Perineurial glia
****
Fed
NR
G
Fed
Lac::GFP
H
NR
I
Fed
SPG Dextran
J
NR
Pixel intensity
Distance (μm)
Pixel intensity
Distance (μm)

Figure 4

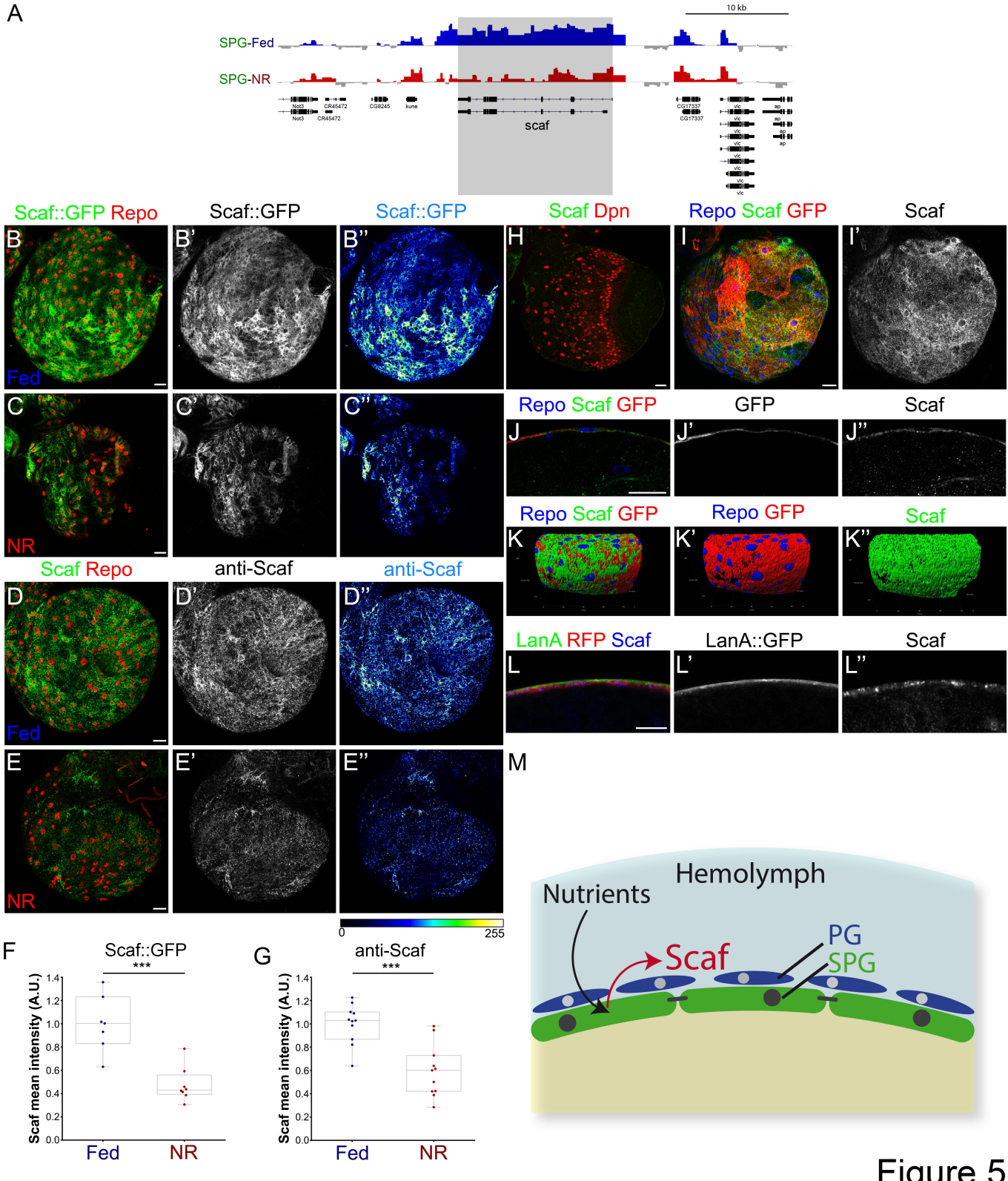
A
10 kb
SPG-Fed
SPG-NR
scaf
Scaf::GFP Repo
Scaf::GFP
Scaf::GFP
Scaf Dpn
Repo Scaf GFP
Scaf
Fed
NR
Repo Scaf GFP
GFP
Scaf
Repo Scaf GFP
Repo GFP
Scaf
Scaf Repo
anti-Scaf
anti-Scaf
LanA RFP Scaf
LanA::GFP
Scaf
0
255
M
Hemolymph
Nutrients
Scaf
PG
SPG
F
Scaf::GFP
***
Scaf mean intensity (A.U.)
Fed
NR
G
anti-Scaf
***
Scaf mean intensity (A.U.)
Fed
NR

Figure 5

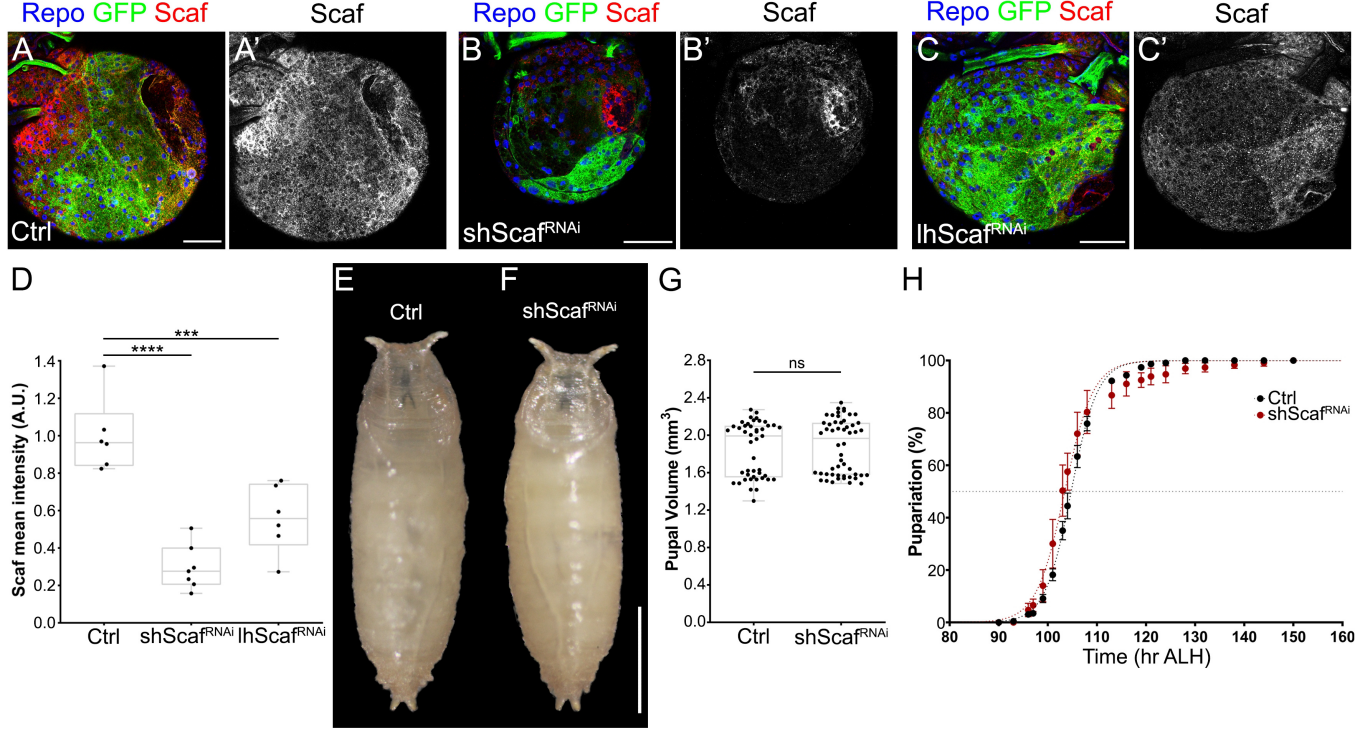
Repo GFP Scaf
Scaf
A
A'
Ctrl
B
B'
shScaf^RNAi
C
C'
lhScaf^RNAi
D
Scaf mean intensity (A.U.)
***
****
Ctrl
shScaf^RNAi
lhScaf^RNAi
E
F
Ctrl
shScaf^RNAi
G
Pupal Volume (mm^3)
ns
H
Pupariation (%)
Time (hr ALH)
Ctrl
shScaf^RNAi

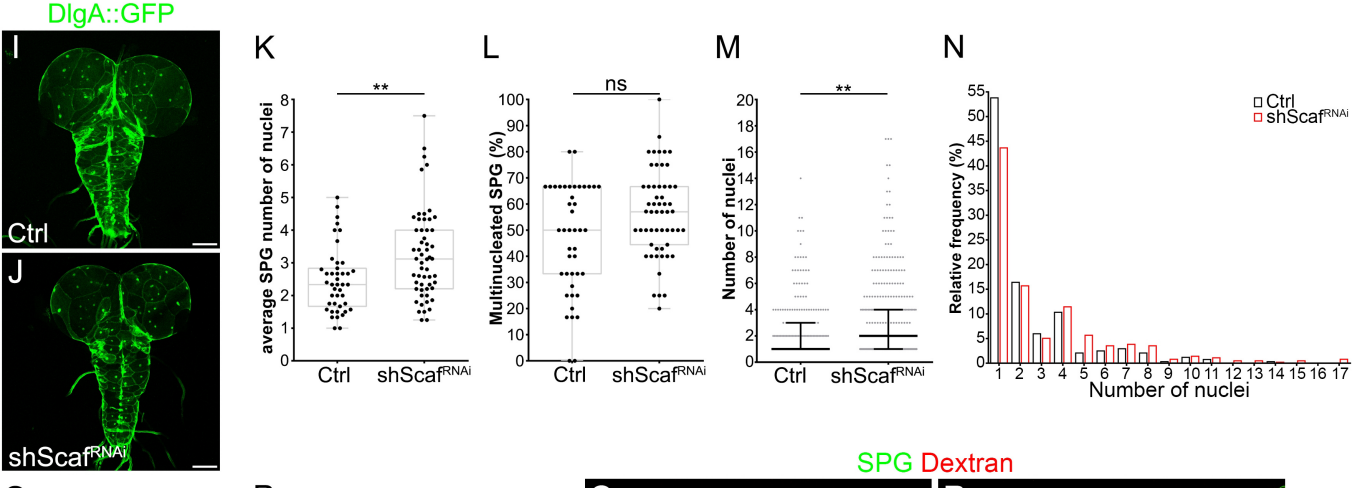
DlgA::GFP
I
Ctrl
J
shScaf^RNAi
K
average SPG number of nuclei
**
L
Multinucleated SPG (%)
ns
M
Number of nuclei
**
N
Relative frequency (%)
Number of nuclei
Ctrl
shScaf^RNAi

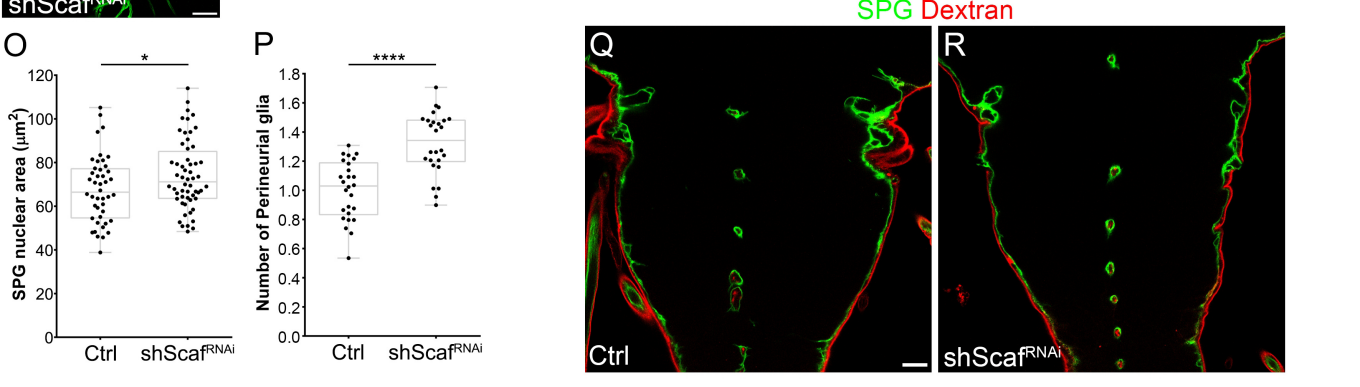
O
SPG nuclear area (μm^2)
*
P
Number of Perineurial glia
****
SPG Dextran
Q
Ctrl
R
shScaf^RNAi

Figure 6

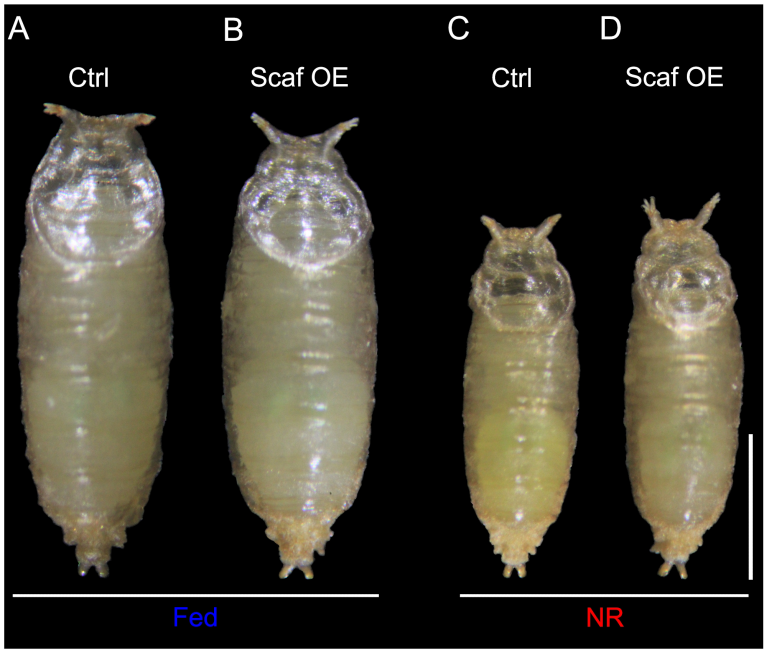
A
B
C
D
Ctrl
Scaf OE
Ctrl
Scaf OE
Fed
NR

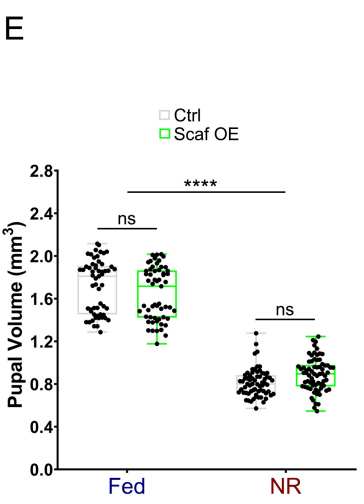
E
Ctrl
Scaf OE
Pupal Volume (mm3)
****
ns
ns
Fed
NR

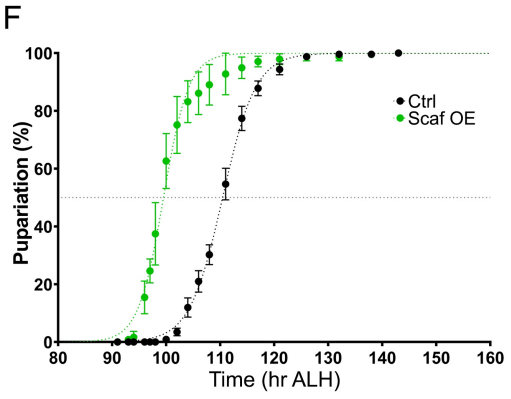
F
Pupariation (%)
Ctrl
Scaf OE
Time (hr ALH)

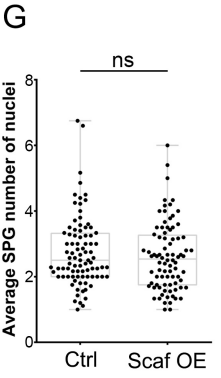
G
Average SPG number of nuclei
ns
Ctrl
Scaf OE

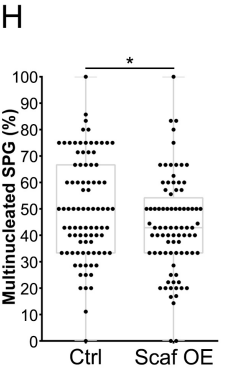
H
Multinucleated SPG (%)
*
Ctrl
Scaf OE

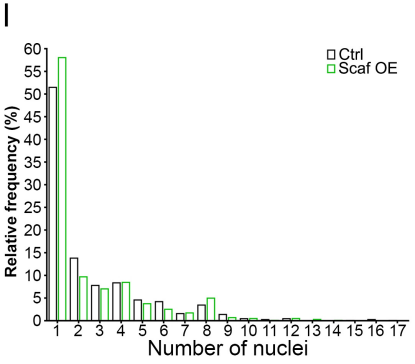
I
Relative frequency (%)
Ctrl
Scaf OE
Number of nuclei

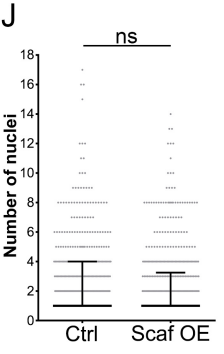
J
Number of nuclei
ns
Ctrl
Scaf OE

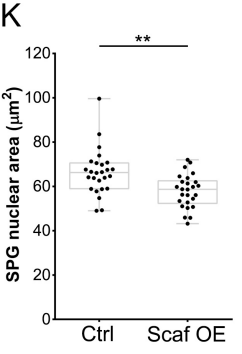
K
SPG nuclear area (μm2)
**
Ctrl
Scaf OE

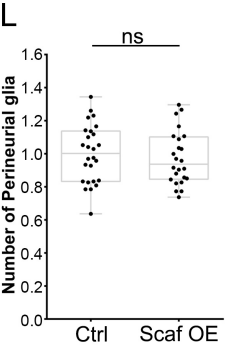
L
Number of Perineurial glia
ns
Ctrl
Scaf OE

Figure 7

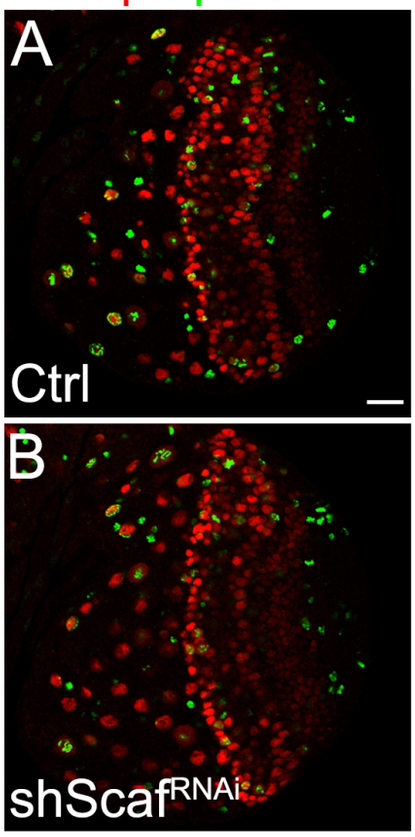
Dpn pH3
A
Ctrl
B
shScaf^RNAi

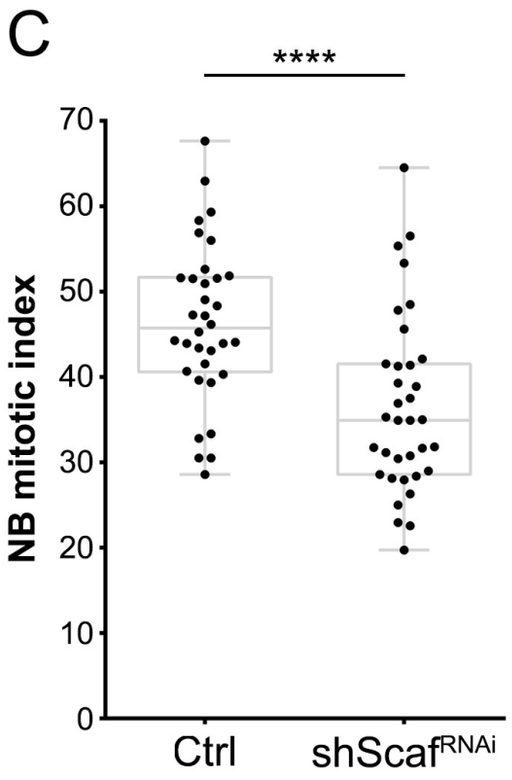
C
****
NB mitotic index
70
60
50
40
30
20
10
0
Ctrl
shScaf^RNAi

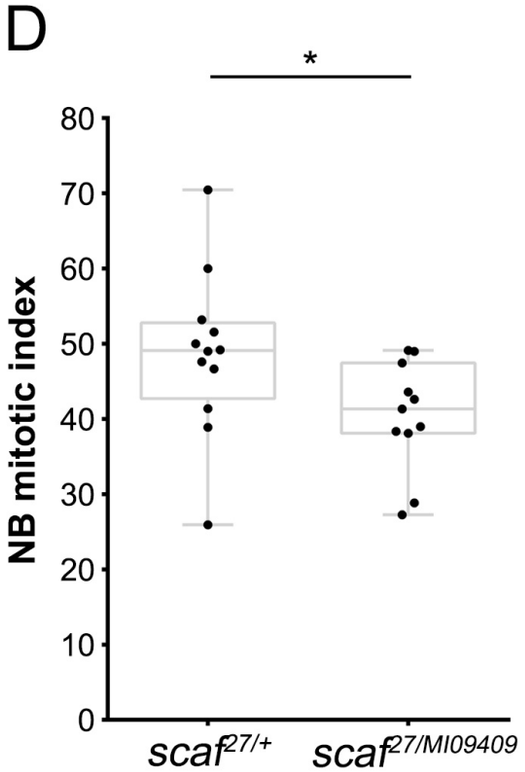
D
*
NB mitotic index
80
70
60
50
40
30
20
10
0
scaf^27/+
scaf^27/MI09409

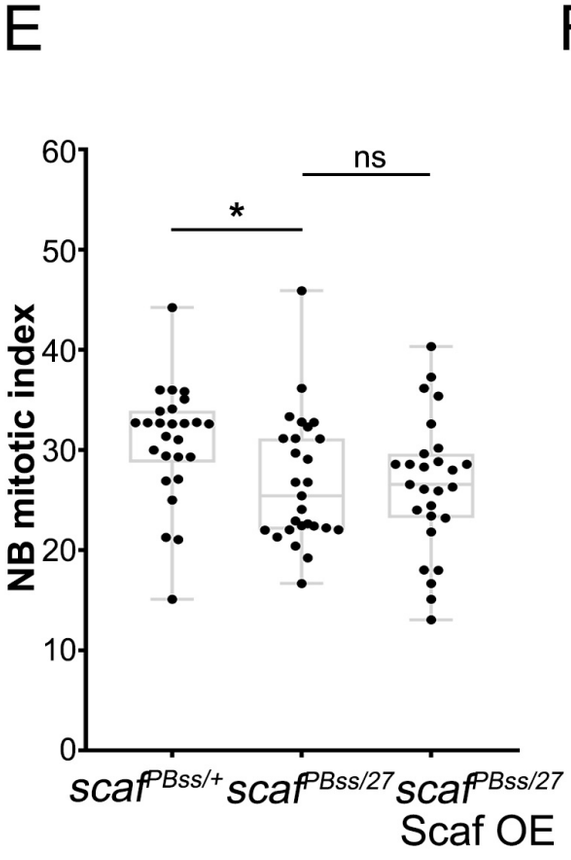
E
ns
*
NB mitotic index
60
50
40
30
20
10
0
scaf^PBss/+
scaf^PBss/27
scaf^PBss/27
Scaf OE

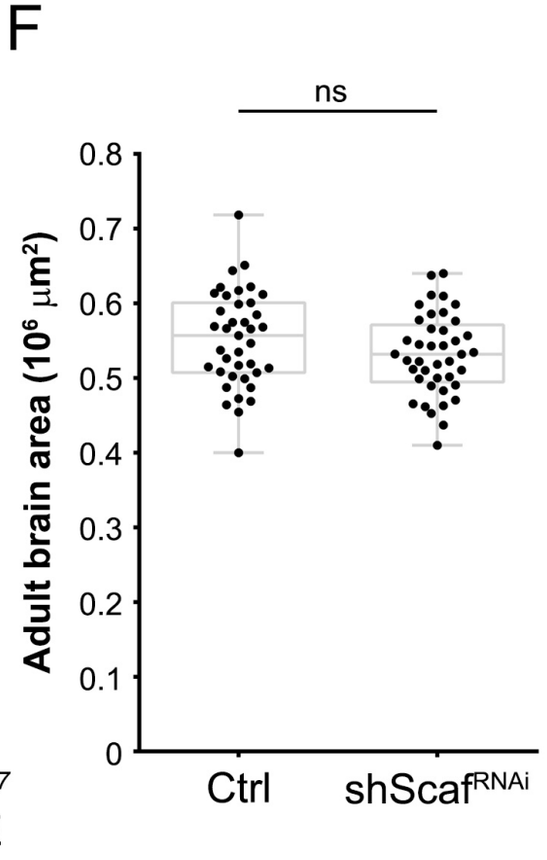
F
ns
Adult brain area (10^6 µm^2)
0.8
0.7
0.6
0.5
0.4
0.3
0.2
0.1
0
Ctrl
shScaf^RNAi

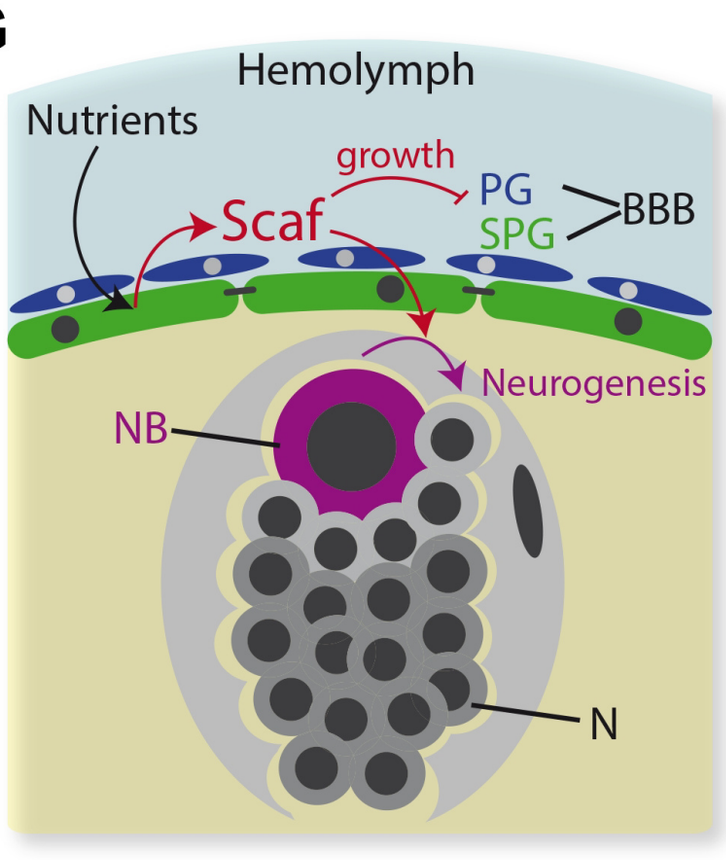
G
Hemolymph
Nutrients
growth
Scaf
PG
SPG
BBB
Neurogenesis
NB
N

Figure 8

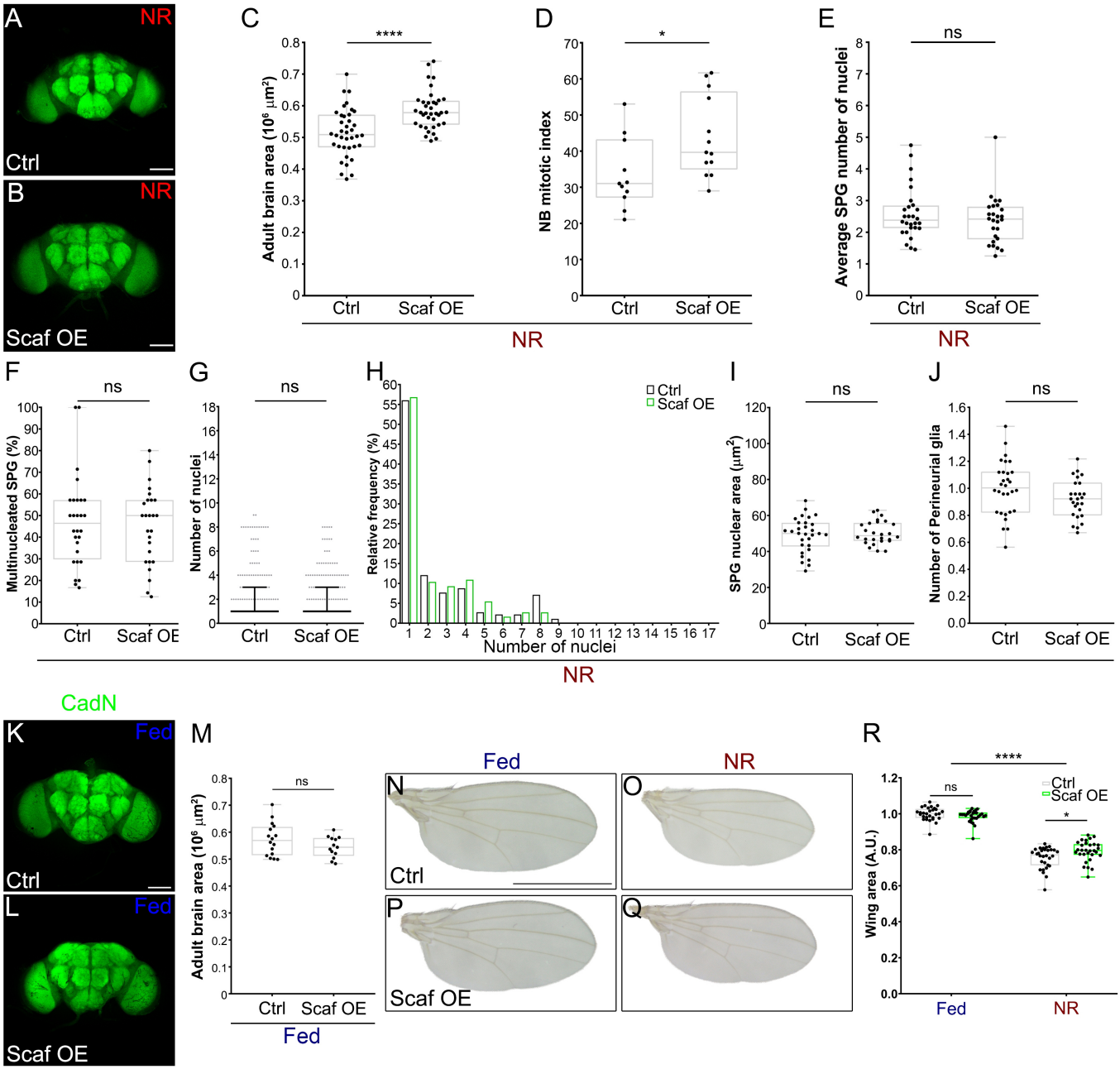
CadN
A
NR
Ctrl
B
NR
Scaf OE
C
****
Adult brain area (10^6 µm^2)
Ctrl
Scaf OE
NR
D
*
NB mitotic index
Ctrl
Scaf OE
E
ns
Average SPG number of nuclei
Ctrl
Scaf OE
NR
F
ns
Multinucleated SPG (%)
Ctrl
Scaf OE
G
ns
Number of nuclei
Ctrl
Scaf OE
H
Ctrl
Scaf OE
Relative frequency (%)
Number of nuclei
I
ns
SPG nuclear area (µm^2)
Ctrl
Scaf OE
J
ns
Number of Perineurial glia
Ctrl
Scaf OE
NR
CadN
K
Fed
Ctrl
L
Fed
Scaf OE
M
ns
Adult brain area (10^6 µm^2)
Ctrl
Scaf OE
Fed
Fed
NR
N
Ctrl
O
P
Scaf OE
Q
R
****
ns
*
Ctrl
Scaf OE
Wing area (A.U.)
Fed
NR

Figure 9

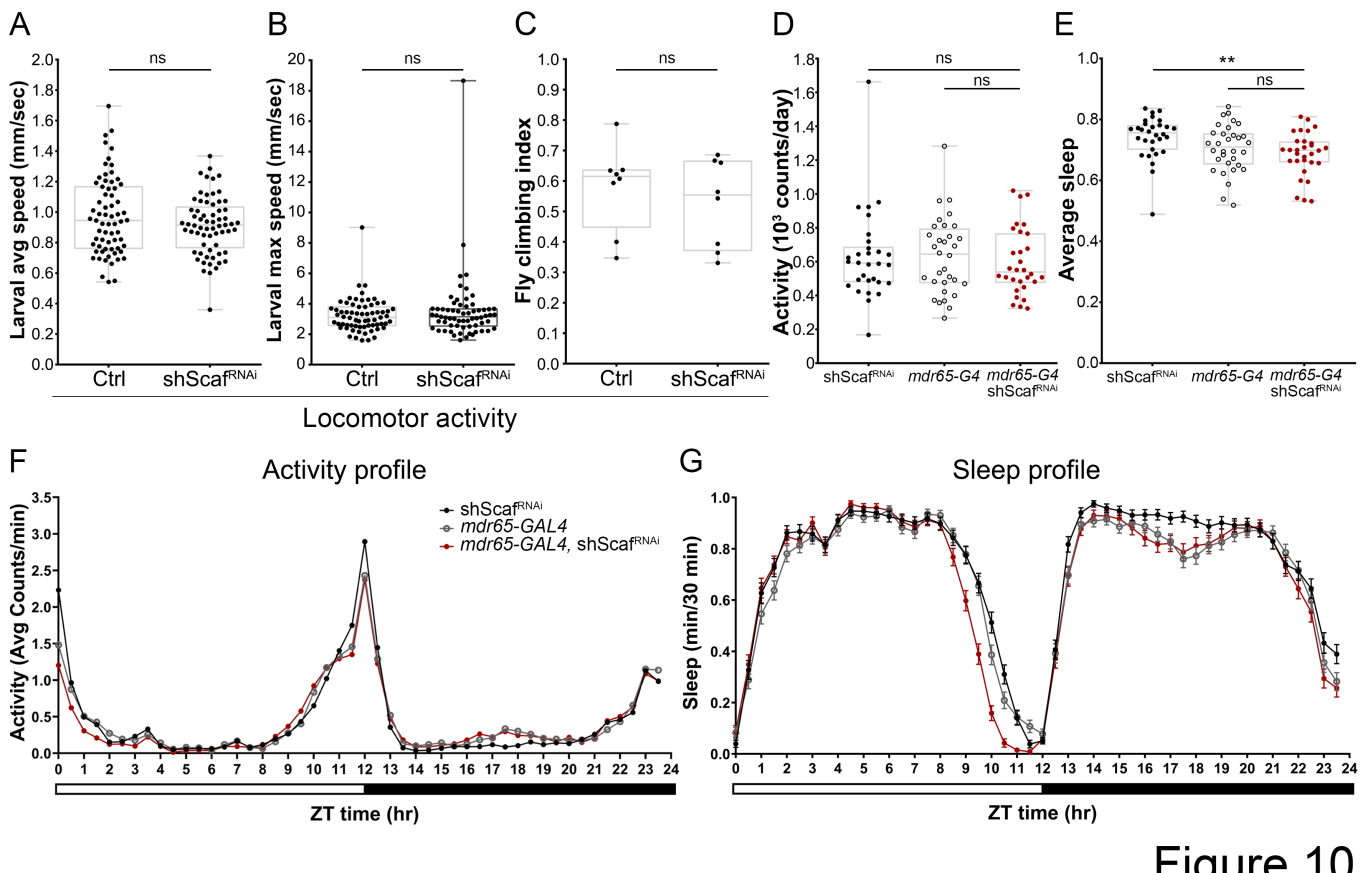
A
B
C
D
E
ns
**
Larval avg speed (mm/sec)
Larval max speed (mm/sec)
Fly climbing index
Activity (10³ counts/day)
Average sleep
Ctrl
shScaf^RNAi
mdr65-G4
mdr65-G4 shScaf^RNAi
Locomotor activity
F
Activity profile
G
Sleep profile
shScaf^RNAi
mdr65-GAL4
mdr65-GAL4, shScaf^RNAi
Activity (Avg Counts/min)
Sleep (min/30 min)
ZT time (hr)

Figure 10

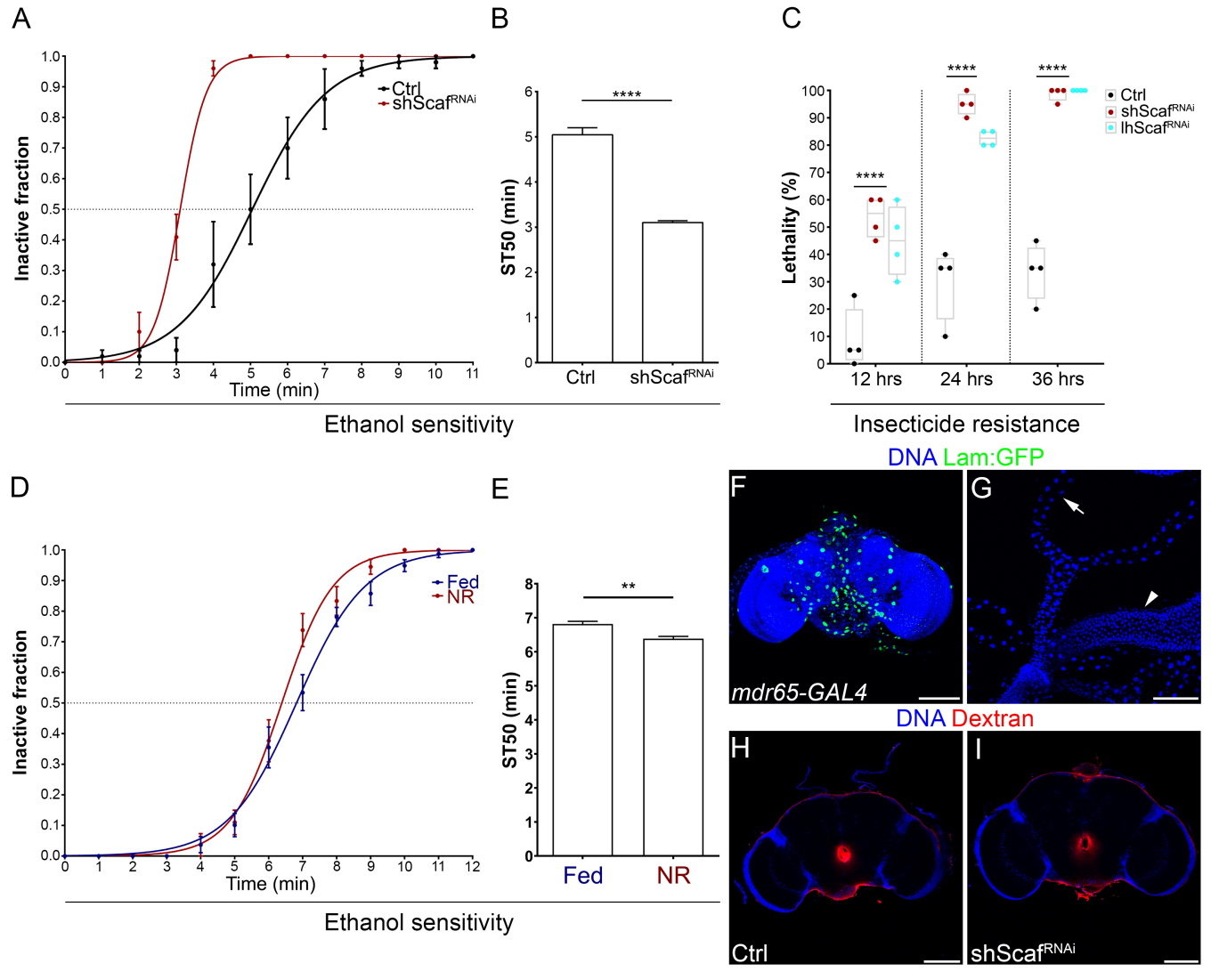
A
Inactive fraction
Time (min)
Ctrl
shScaf^RNAi
B
ST50 (min)
****
Ctrl
shScaf^RNAi
Ethanol sensitivity
C
Lethality (%)
****
****
****
Ctrl
shScaf^RNAi
lhScaf^RNAi
12 hrs
24 hrs
36 hrs
Insecticide resistance
D
Inactive fraction
Time (min)
Fed
NR
E
ST50 (min)
**
Fed
NR
Ethanol sensitivity
DNA Lam:GFP
F
mdr65-GAL4
G
DNA Dextran
H
Ctrl
I
shScaf^RNAi

Figure 11

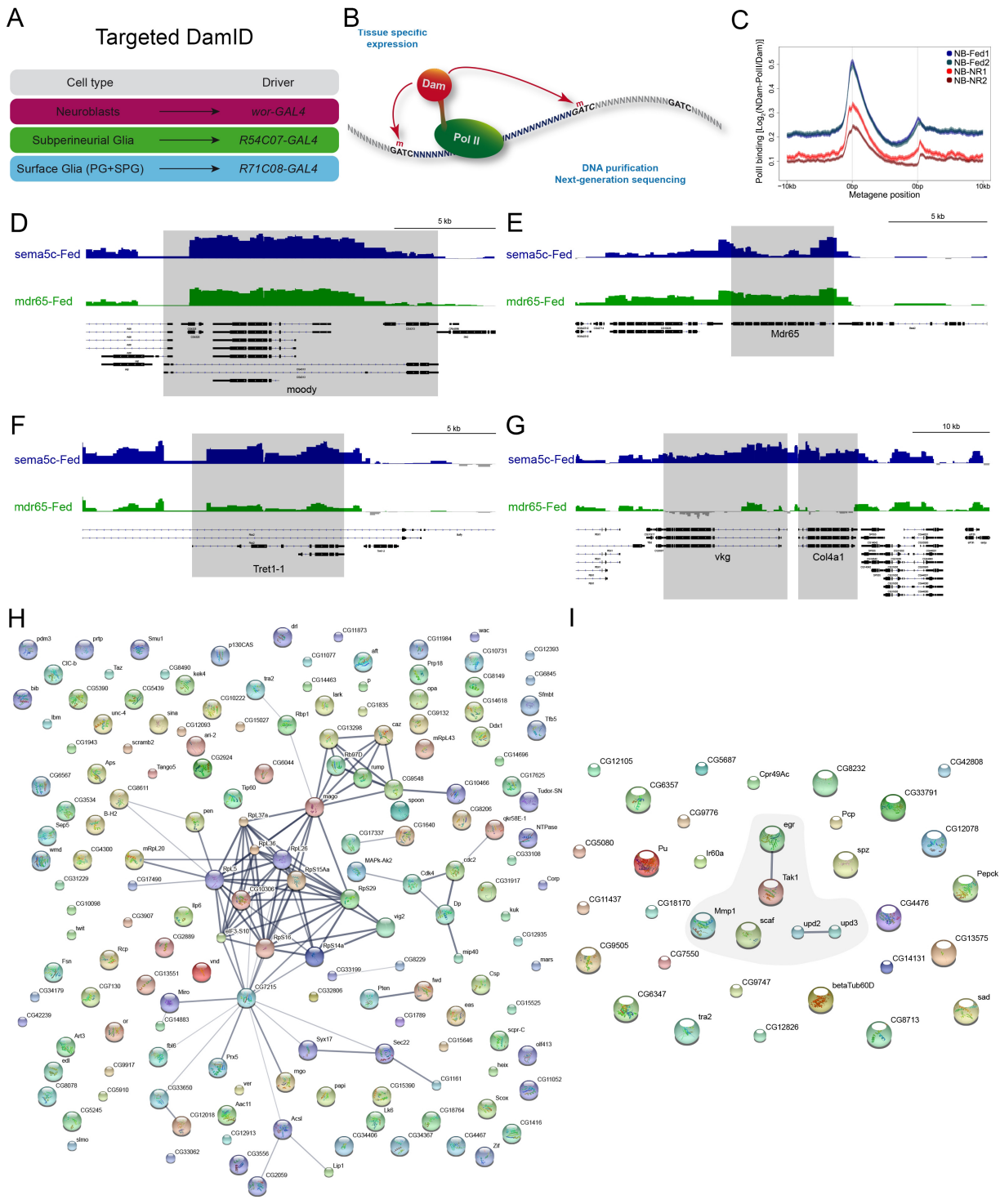
A
Targeted DamID
Cell type
Driver
Neuroblasts
wor-GAL4
Subperineurial Glia
R54C07-GAL4
Surface Glia (PG+SPG)
R71C08-GAL4
B
Tissue specific expression
Dam
Pol II
DNA purification
Next-generation sequencing
C
NB-Fed1
NB-Fed2
NB-NR1
NB-NR2
PolII binding [Log2(NDam-PolII/Dam)]
Metagene position
D
sema5c-Fed
mdr65-Fed
5 kb
moody
E
sema5c-Fed
mdr65-Fed
5 kb
Mdr65
F
sema5c-Fed
mdr65-Fed
5 kb
Tret1-1
G
sema5c-Fed
mdr65-Fed
10 kb
vkg
Col4a1
H
I
egr
Tak1
Mmp1
scaf
upd2
upd3
Pcp
spz
Pu
Ir60a

Figure 2-1

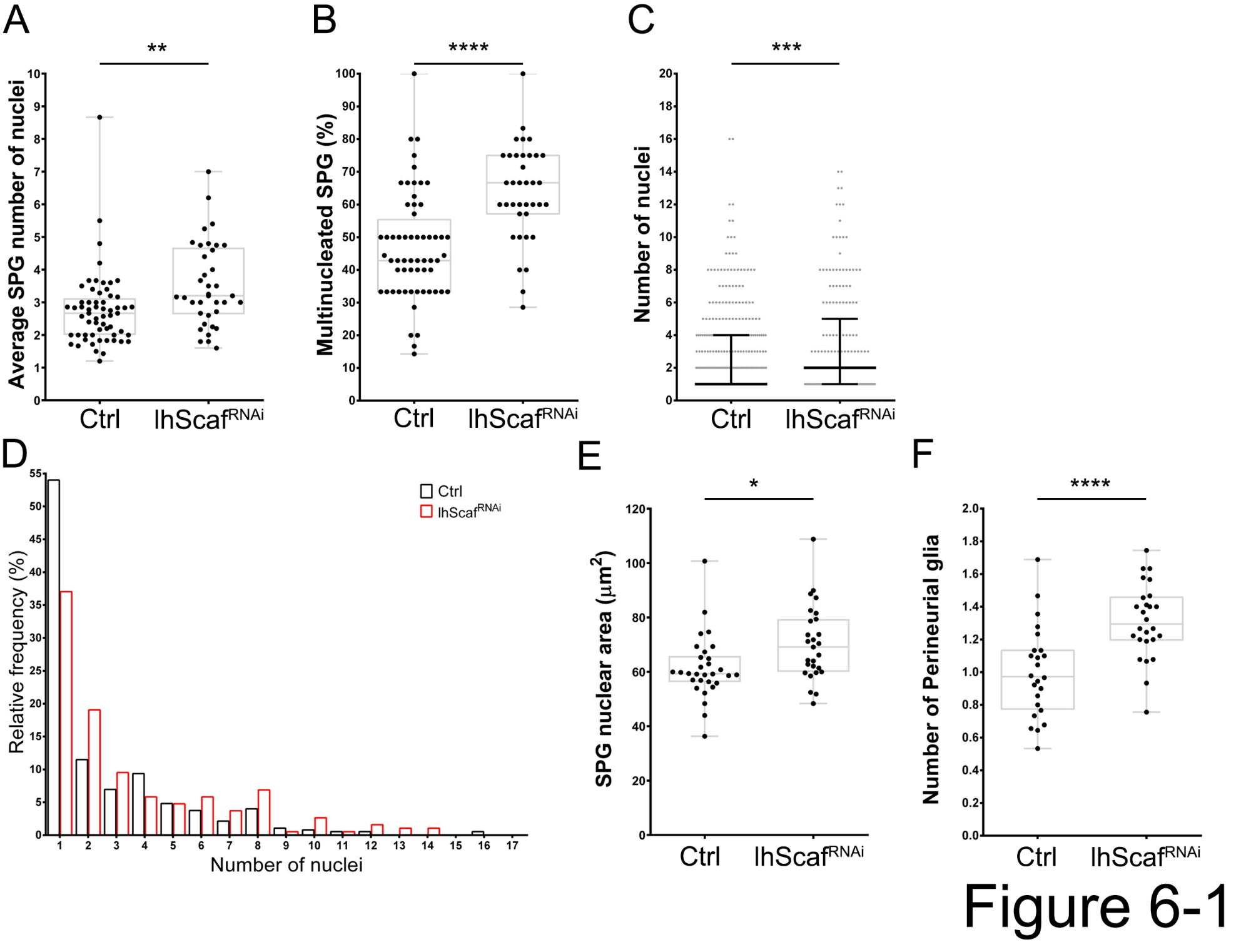
A
**
Average SPG number of nuclei
Ctrl
lhScaf^RNAi
B
****
Multinucleated SPG (%)
Ctrl
lhScaf^RNAi
C
***
Number of nuclei
Ctrl
lhScaf^RNAi
D
Ctrl
lhScaf^RNAi
Relative frequency (%)
Number of nuclei
E
*
SPG nuclear area (μm²)
Ctrl
lhScaf^RNAi
F
****
Number of Perineurial glia
Ctrl
lhScaf^RNAi

Figure 6-1